U. of Iowa 70:55

N71-16339

NASA CR116143

PLASMA IN THE EARTH'S POLAR MAGNETOSPHERE

by

L. A. Frank

Department of Physics and Astronomy

THE UNIVERSITY OF IOWA

Iowa City, Iowa

U. of Iowa 70-55

PLASMA IN THE EARTH'S POLAR MAGNETOSPHERE

by

L. A. Frank

November 1970

Department of Physics and Astronomy
The University of Iowa
Iowa City, Iowa 52240

* Research supported in part by the National Aeronautics and Space Administration under contract NAS5-9074.

Abstract

First observations of the plasmas in the dayside polar magnetosphere were obtained with the earth-satellite IMP 5 during July - August 1969. Several of the more important observational results are:

- the polar neutral 'points' which appear at the high-latitude magnetopause in mathematical models for the shape of the geomagnetic cavity formed by the interaction of the solar wind with the geomagnetic field are observationally 'bands' with width $\sim$ 1 R_E across the dayside high-latitude magnetopause (one 'band' in the Northern hemisphere and presumably a second in the Southern hemisphere),

- these two 'bands', or regions of the magnetopause through which the magnetosheath plasma has direct access to the magnetosphere, and the corresponding extension of these bands from magnetopause to auroral altitudes have been designated herein as the 'polar cusps',

- at all other positions of the dayside magnetopause, the magnetopause appears to be an effective barrier against the direct entry of magnetosheath plasma,

- during periods of relative magnetic quiescence the intersection of the dayside polar cusp with the auroral zone is positioned at invariant latitude $\Lambda = 79° (\pm 1°)$ and its latitudinal width is 10 to 30 km projected onto the auroral zone,

- during periods of relative magnetic disturbance the position of the polar cusp moves equatorward by several degrees in invariant latitude without a large increase in its latitudinal width, i.e., by factors ≤ 2.

- the high-latitude termination of energetic trapped electron (E > 45 keV) intensities in the high-latitude dayside outer radiation zone occurs coincident with the polar cusp, albeit these intensities are small and of irregular profile with radial distance in this region,

- no measurable intensities of energetic electrons (E > 40 keV), magnetosheath protons and electrons, and ring-current protons were observed at latitudes above the polar cusp, i.e., in the polar cap region,

- the proton and electron differential energy spectrums as viewed in the solar direction in the distant polar cusp (within several earth radii of the magnetopause) are identical to those observed within the magnetosheath to within observational accuracy,

- the bulk velocity of protons in the distant polar cusp as deduced from the angular distributions appears to be lower than that of the magnetosheath plasma near the magnetopause by factors $\sim$ 2 or 3,

- in the mid-altitude polar cusp at $\sim$ 4 to 5 R_E geocentric radial distances, the proton spectrum differs from that at the magnetosheath in that protons with energies $\leqslant$ 500 eV are severely less than those observed in the magnetosheath,

- the proton spectrums in the mid-altitude polar cusp are similar to those in the distant plasma sheet with the exception that the proton number densities in the polar cusp are typically larger by factors $\sim$ 20 to 200,

- the angular distributions of proton intensities in the mid-altitude polar cusp are strongly peaked along the local magnetic field (i.e., down into the auroral zone); the dimensions of the atmospheric loss cone at these altitudes appear to be insufficiently large to account for the observed anisotropy, and

- the magnetosheath plasma in the mid-altitude polar cusp is observed to be separated into two thin sheets, one of magnetosheath proton intensities and the other populated with magnetosheath electrons; these sheets are immediately adjacent to each other with the electron sheet equatorward of the proton sheet; their latitudinal widths as projected into the auroral zone are roughly equal, $\sim$ 10 to 30 km.

These observations, along with recent measurements from other earth-satellites, have been interpreted in terms of a proposed magnetospheric model with several new features, among which are:

- plasma sheet protons gain access to the magnetosphere via the dayside polar cusps,
- all magnetic field lines threading the distant plasma sheet beyond $\sim$ 10 or 12 R_E were convected from the polar cusps, and
- magnetic field lines in the polar cap region of the magnetotail do not merge or pass through the plasma sheet.

I. Introduction

Over these past ten years or so after the initial surveys, near the magnetic equatorial plane and at low altitudes, of the vast radiation zones encircling the earth, it has often been suggested that measurements of charged particles and magnetic fields in the distant polar magnetosphere would yield several decisive conclusions concerning the sources of the auroral corpuscular radiations and of the topology of the distant geomagnetic field. First such observations of plasmas in the distant polar magnetosphere are reported here.

The interaction of the earth's dipole magnetic field with a stream of solar plasma was first considered by Chapman and Ferraro [1931; see also Chapman, 1960]. In this two-dimensional approximation a plane sheet of plasma (electromagnetically an infinite plate with infinite conductivity) oriented parallel to the earth's magnetic moment was moved toward the dipole. An interesting feature of the subsequent distortion of the geomagnetic field is the presence of two 'neutral points' with $\vec{B} = 0$ at the sheet surface. In more recent years the three-dimensional problem has been undertaken

(see the review by Spreiter et al [1968] for a comprehensive summary and bibliography). Again a pair of neutral points, one each in the high latitudes of the Northern and Southern hemispheres, occurs and represents the intersections of two interior magnetic field lines with the cavity surface (magnetopause). All field lines on the magnetopause converge to the northern neutral point and diverge from the southern neutral point. In the principal meridional plane, local noon-midnight, the field lines located at latitudes higher than the neutral point are assumed to be swept back into the geomagnetic tail and field lines at latitudes below the neutral point pass through the sunlit hemisphere of the geomagnetic cavity.

An obvious question arises: Can solar plasma flow directly into the geomagnetic cavity through these polar neutral points? This relatively simple query may be followed with a host of further speculations relating these neutral points to auroral and magnetospheric phenomena. However, until now no satellite has penetrated the distant polar magnetosphere at sufficiently high magnetic latitudes to provide a useful survey of this region. Of course, observations from literally a swarm of low-altitude polar satellites

instrumented with plasma and energetic particle detectors has been used to survey the polar cap regions at altitudes $\sim$ several thousand kilometers for evidences of a direct influx of magnetosheath plasma via the neutral points. These searches have been largely unsuccessful, perhaps due to inadequate temporal and energy resolutions of the instruments and the difficulties of identifying these particle influxes amidst the complex precipitation patterns over the auroral zone.

Within the past year two series of measurements of direct influxes of magnetosheath plasma to low altitudes have been reported. Heikkila and Winningham [1970] have observed electron and proton intensities similar to those of the magnetosheath over a broad latitude segment, $\sim$ several degrees in magnetic latitude, of the dayside auroral zone during a large magnetic storm. A much narrower band of magnetosheath plasma, $\sim$ 50 km or $\sim$ a few tenths of a degree in magnetic latitude, located at the high-latitude boundary of the dayside auroral precipitation pattern has recently been identified as the low-altitude signature of the polar neutral point [Frank and Ackerson, 1970]. In fact since this band is observed over a large range of local times over

the sunlit auroral zone, the 'neutral point' at the magnetopause is a 'neutral line' across the high-latitude magnetopause.

The first in situ observations of the character of the plasmas in the vicinity of this neutral line at the high-latitude dayside magnetopause are summarized here. These results are interpreted in terms of a proposed magnetospheric model which identifies the geomagnetic field lines threading the polar cusp of plasmas found in the vicinity of the neutral point with the field lines in the distant plasma sheet via a convection of field lines from polar cusp to plasma sheet. This model predicts, for example, that the intersection of all field lines through the plasma sheet beyond $\sim$ 10 or 12 R_E (earth radii) onto the auroral zone during periods of relative magnetic quiescence occurs at the high-latitude boundary of the nighttime auroral precipitation patterns and has a latitudinal width of $\leqslant 1°$.

II. Instrumentation

The observations of low-energy plasma in the polar magnetosphere reported here were gained with two electrostatic analyzer arrays borne on the earth-satellite IMP 5. This spacecraft was launched on 21 June 1969 into a highly eccentric orbit with initial apogee and perigee geocentric radial distances of 28.8 R_E and 1.05 R_E, respectively, an inclination of 86.8° and a period of 3.4 days. At launch the sun-earth-apogee angle was 2°. The spin axis of the spacecraft was oriented nearly perpendicular to the ecliptic plane with a spin-axis-sun angle of 92°. The fields-of-view of the two plasma detectors were directed perpendicular to this spin axis. Responses of each detector were serviced by accumulators and sample-and-hold circuits with sufficient temporal resolution to obtain angular distributions of the low-energy charged particle intensities during the spin period of the spacecraft, $\sim$ 2 seconds.

The two plasma instruments were a Low-Energy Proton and Electron Differential Energy Analyzer (abbreviation, LEPEDEA) and a solar wind ion detector. The LEPEDEA provided simultaneous measurements of the directional,

differential intensities of protons and electrons over the energy range $80 \leqslant E \leqslant 50{,}000$ eV in sixteen essentially contiguous energy bandpasses. Angular distributions were obtained by accumulating the responses of the detectors for a period corresponding to approximately 55° of satellite rotation. The spacecraft solar aspect detector yielded the necessary information for calculations of the corresponding directions for each of the above angular sectors. Detailed descriptions of this electrostatic analyzer have been previously published [Frank, 1967a,b, 1970a; Frank et al, 1969].

The second plasma instrument, a solar wind ion detector, is essentially a modified LEPEDEA with improved energy resolution $\Delta E/E = 0.06$ and with a narrower field-of-view, $\sim 5°$, in the plane of the ecliptic. This instrument was capable of positive ion measurements only. The dimensions of the fields-of-view for both this instrument and the LEPEDEA were 30° in the plane containing the spin axis and the axis of the field-of-view of each detector, i.e., perpendicular to the ecliptic plane. The solar wind ion detector covered the energy range $91 \leq E \leq 12{,}300$ eV with 32 energy, or E/Q, bandpasses. These energy bandpasses were not contiguous, in contrast to those of the LEPEDEA which

is endowed with significantly wider bandpasses $\Delta E/E \simeq 0.5$. Measurements of the angular distributions of ion intensities in fifteen angular segments in the ecliptic plane for each of sixteen energy bandpasses and in seven angular segments for all thirty two bandpasses were telemetered. The effective angular width of each of these 'buckets' was 6.5°. The seven common angular sectors were closely grouped near the solar direction; and the remaining eight sectors were positioned at large angles to the solar direction for measurements of ion angular distributions in the magnetosheath.

III. A Typical Series of Observations in the Dayside Magnetosphere.

The responses of the LEPEDEA and the solar ion detector for a pair of typical inbound and outbound passes through the dayside magnetosphere are presented here to orient the reader as to the geometry of the satellite orbit and the nature of the regions encountered. Generally speaking, outbound passes were located near the magnetic equator and inbound passes traversed the polar magnetosphere.

Typical directional intensities of electrons and protons for an outbound pass on 11 July 1969 near local noon are shown in Figure 1. Selected spatial coordinates are summarized in Figure 2. The corresponding angular quadrant for the directions of the fields-of-view which has been chosen here is $225° \leq \phi_{SE} \leq 315°$ where ϕ_{SE} is the spacecraft-centered solar ecliptic longitude of the field-of-view. This angular range has been chosen since it provides an unambiguous identification of such regions as the interplanetary medium, magnetosheath and the magnetopause. In Figure 1 the outer radiation zone is clearly identified by the large intensities of electrons $E > 45$ keV extending

to the magnetopause located at 71,000 km and by the proton ($12 \leq E \leq 19.5$ keV) intensities of the extraterrestrial ring current (bottom of Figure 1). The intensities of protons ($690 \leq E \leq 1100$ eV) at large angles to the solar direction as shown at the top of Figure 1 provide an effective signature for the magnetosheath. Note that the severe termination of trapped energetic electron ($E > 45$ keV) intensities at the magnetopause is coincident with a similar decrease in ring current proton intensities and that there is a relative absence of any significant lower-energy proton ($690 \leq E \leq 1100$ eV) intensities characteristic of the magnetosheath inside the position of the magnetopause. Observationally the magnetopause near the magnetic <u>equatorial</u> plane appears to be an extremely effective barrier against the direct entry of solar plasma.

A similar series of measurements of proton and electron intensities for the inbound pass of the satellite on 11 July through the dayside <u>polar</u> magnetosphere is presented in Figure 3. Appropriate coordinates such as dipole magnetic latitude λ_m and solar magnetospheric longitude ϕ_{sm} as functions of geocentric radial distance are summarized in Figure 2. For the radial distance range $17,000 \leq R \leq 40,000$ km

the geomagnetic latitude of the satellite position is $\geq 60°$. Of immediate attention is the occurrence of an intense narrow band of proton ($690 \leq E \leq 1100$ eV) intensities centered at 34,000 km which are similar to those found within the magnetosheath (see top panel of Figure 3). The corresponding magnetic latitude is 68° and the magnetic shell parameter $L \simeq 40$. This narrow region in the dayside magnetosphere to which the magnetosheath plasma (explicitly, the low-energy protons) has direct access is designated herein as the polar cusp. Other important features of the plasmas in the polar magnetosphere as displayed in Figure 3 are

- the polar cap region at $R \leq 33{,}000$ km within which are no measurable intensities of energetic electrons ($E > 45$ keV), ring current protons ($12 \leq E \leq 19.5$ keV) or magnetosheath protons ($690 \leq E \leq 1100$ eV),
- the high-latitude outer radiation zone, $36{,}000 \leq R \leq 64{,}000$ km, with energetic electron ($E > 45$ keV) intensities terminating at the position of the polar cusp and with the magnitudes of intensities considerably less than those measured at the equator (cf. Figure 1),
- measurable intensities of protons ($12 \leq E \leq 19.5$ keV) of the extraterrestrial ring current throughout the region of the high-latitude outer radiation zone, and
- relatively low intensities of low-energy protons ($690 \leq E \leq 1100$ eV), presumably of magnetosheath origin, just inside the magnetopause and outside of the polar cusp in the outer zone.

Again, as at the magnetic equator, the high-latitude magnetopause appears to be an effective barrier against direct entry of magnetosheath plasma into the magnetosphere with the exception of the narrow region designated here as the polar cusp. The coordinates for these observations of the polar cusp are labelled (PC) in Figure 2. A further summary of the positions of the various regions for both inbound and outbound passes as functions of geocentric radial distance and dipole magnetic latitude λ_m is given in Figure 4.

IV. Observations of the Spatial Distributions and Energy Spectrums of Plasma in the Polar Cusp

We have examined twelve consecutive series of measurements such as those discussed in the previous section and eleven of the inbound passes crossed the polar cusp. No telemetry was available for the twelfth traversal. Hence, the polar cusp is a permanent, not transitory, feature of the polar magnetosphere. Further, since the satellite traversed the polar cusp over a relatively wide range of local times in the dayside magnetosphere its intersection with the magnetopause must be a line, or band, across the high latitude magnetopause, not a point. This intersection is designated here as the 'neutral band' since as we shall show, the width of this intersection of the polar cusp with the magnetopause in the principal meridional plane is $\sim 1\ R_E$.

Our discussion of the observations which follows below is a brief summary of the more important features of the polar cusp.

Spatial configuration.

A detailed tabulation of coordinates and Universal Times for encounters with the polar cusp during eleven inbound passes through the polar magnetosphere is given in Appendix. In order to obtain the geometry of the polar cusp, say, in R - λ_m coordinates, both temporal variations of the position of the polar cusp and the effects of differing angles of attack of the solar wind must be determined. A summary of all eleven crossings of the polar cusp is shown in Figure 5. The coordinates are geocentric radial distance and dipole invariant latitude $\Lambda = \text{Cos}^{-1} \left(\frac{1}{L}\right)^{1/2}$. We have chosen Λ over shell parameter L and magnetic latitude λ_m since L is rather cumbersome in the polar magnetosphere and λ_m does not readily identify the latitude of the intersection of the field line with the earth. However, the R - λ_m coordinate system will be employed later to display the geometry of the polar magnetosphere. Noteworthy features of Figure 5 are

- Λ increases with increasing geocentric radial distance, i.e., the magnetic field is distorted in such a manner that the field lines are bent in the antisolar direction relative to the unperturbed dipole field,

- the broadening of the cusp with increasing geocentric radial distance,
- the movement of the polar cusp to lower latitudes during three of the five periods of relative magnetic disturbance (a feature which will be discussed with respect to magnetic substorms in a later report),
- the above movement of the polar cusp is not accompanied by a severe increase in the width of the cusp, $\leq$ a factor of two (i.e., the primary effect of increased magnetic activity appears to be a movement equatorward), and
- the intersection of the polar cusp with the auroral zone during periods of relative magnetic quiescence is positioned at $\Lambda = 79° (\pm 1°)$.

In determining the position of the polar cusp as a function of R and Λ during quiescent periods we have excluded all measurements for which $K_p \geq 2$. The corresponding average position is given in Figure 5 (dashed line). However, we have not yet discussed the effects of the correlation of the angle of attack of the solar wind with respect to the direction of the earth's magnetic moment and the geocentric radial distance for encounter of the polar cusp. If there were no such correlation, i.e., the position of the cusp is determined only by the direction of solar wind flow, all of the polar cusp crossings would occur at nearly the same radial distance. Inspection of Figure 5 clearly shows that this is not the case. In order to further

estimate the effect of the changing angle of attack, or differing Universal Times for polar cusp crossings from pass to pass, we have invoked the calculations of Spreiter and Briggs [1962] for the expected positions of the neutral points on the magnetopause for the two observational extremes of the angles of attack, $\lambda = 10°$ and $35°$, during our period. The results of their calculations in R - Λ coordinates are shown in Figure 6 for (1) radial distance to neutral point = 8.6 R_E and (2) radial distance to magnetopause perpendicular to dipole moment = 11 R_E. The maximum calculated variation of $\Delta\Lambda \simeq 1.5°$ at the magnetopause represents the extreme, i.e., at smaller radial distances $\Delta\Lambda$ is smaller. On the basis of the above discussion we conclude that the variation of the invariant latitudes of the polar cusp crossings with geocentric radial distance is dominantly the signature of the spatial configuration of the polar cusp in geomagnetic coordinates and, to a considerably lesser degree, the result of the variations in the angle of attack of the solar wind.

In Figure 6 the positions of the polar cusp in the Mead-Williams [Roederer, 1968] and Hones-Taylor [Antonova and Shabansky, 1968] models for the distant magnetosphere

are compared with the observational result. The Mead-Williams model predicts the polar cusp position to within our observational accuracy. For the convenience of the reader we have summarized all of the results given in Figure 6 in the geocentric radial distance-dipole magnetic latitude ($R - \lambda_m$) grid of Figure 7.

A 'roadmap' for six inbound passes through the polar magnetosphere during periods of relative magnetic quiescence is presented in Figure 8. This diagram gives the geocentric radial distances for each region encountered: interplanetary medium, magnetosheath, outer radiation zone, polar cusp and polar cap region. These passes have been ordered according to the magnetic latitude of the orbit at 4.8 R_E with passes at lowest latitudes appearing at the top of Figure 8. Invariant latitudes Λ ranged from 77.8° to 86.2° for these series of observations. The position of the polar cusp is located at larger radial distances with increasing magnetic latitude of the inbound trajectory. During Revolution 9, for example, the latitude was sufficiently high to allow passage of the satellite directly from the magnetosheath into the polar cusp.

The observations of the polar cusp and its environs in the noon meridional plane are summarized in a R - λ_m coordinate system in Figure 9. Several selected satellite trajectories during periods of relative magnetic quiescence have also been included. It is useful to cross-reference this summary of the polar cusp geometry with the 'roadmap' of Figure 8. As we have mentioned earlier the polar cusp moves equatorward by several degrees in invariant latitude without a large change in latitudinal dimensions at mid-altitudes during periods of relative magnetic disturbance. Inspection of Figures 5, 6, and 7 provides evidence that the intersection of the polar cusp with the magnetopause could occasionally occur at magnetic latitudes λ_m as low as 45° to 50°.

Proton energy spectrums.

In the following discussion we shall consider low-energy charged particle distributions for two types of crossings of the polar cusp, mid-altitude and distant crossings. Revolutions 5 (in) and 9 (in) of Figure 9 provide mid-altitude and distant crossings, respectively. Directional, differential intensities of protons in the magnetosheath and distant polar cusp for Revolution 4

(see Figures 8 and 9) are compared in Figure 10. The direction of the field-of-view of the solar wind ion detector is in the solar direction, $\phi_{SE} = 0°$. These spectrums are essentially identical, considering the known overall variability of intensities in the magnetosheath. In fact it is necessary to utilize the observations of the angular distribution of intensities or the onboard magnetometer responses to distinguish between the two regions. Confirmation of this identification with in situ magnetic field measurements has been accomplished [D. Fairfield, private communication].

The proton differential energy spectrums at mid-altitudes differ from the above proton spectrums in the distant polar cusp. The proton spectrums for the mid-altitude cusp and the magnetosheath for Revolution 6 are shown in Figure 11. These spectrums differ in that the polar cusp spectrums are depleted with respect to protons with energies $\leq$ 500 eV. The polar cusp appears to act on the magnetosheath plasma as a 'velocity filter' by excluding the lower energy protons. For comparison we have included in Figure 11, a typical proton spectrum obtained with IMP 4 in the distant plasma sheet at 33.5 R_E. The mid-altitude polar cusp and

plasma sheet proton spectrums are remarkably similar, with the exception that the polar-cusp proton density is typically larger by factors $\sim$ 20 to 200.

Proton angular distributions.

The angular distributions of low-energy proton intensities in the distant polar cusp and the magnetosheath as measured with the solar ion detector during Revolution 4 are compared in Figure 12. The magnetosheath proton angular distribution at 445 eV has a narrower maximum relative to the polar cusp intensities possibly indicating a lower bulk velocity in the distant polar cusp relative to that of the magnetosheath plasma at the magnetopause. The proton density corresponding to the polar cusp spectrum was larger than that for the magnetosheath spectrum by a factor of 2.3.

The angular distributions typically found in the mid-altitude polar cusp are similar to that shown for Revolution 10 in Figure 13. Proton intensities at 821 eV as measured with the solar ion detector are plotted as functions of local dipole pitch angle α_d. At 4.5 R_E, the direction of the geomagnetic field should not be largely distorted by the solar wind interaction and these calculated directions should be sufficiently accurate relative to the dimensions of the detector field-of-view. The angular distributions are severely peaked at large pitch angles, i.e., the protons

are literally flowing down the magnetic field toward the earth's atmosphere. The size of the backscattered loss cone at these altitudes is indicated in Figure 13. This loss cone is inadequately large to produce the anisotropy over $45° \leqslant \alpha_d \leqslant 135°$ in the observed angular distribution. These angular distributions further stress the high degree of direct access into the magnetosphere that the magnetosheath plasma gains through the dayside polar cusps.

Electron energy spectrums.

The extreme variability of the electron differential energy spectrums in the magnetosheath and distant polar cusp relative to those of the proton spectrums yields a comparison of these electron intensities somewhat more difficult. Examples of the highest- and lowest-intensity spectrums in the distant polar cusp and within the magnetosheath as observed during Revolution 4 are shown in Figure 14. For all practical purposes the electron spectrums measured in these two regions are identical.

A comparison of the electron differential energy spectrums in the polar cusp at mid-altitudes, the high-latitude outer zone and the magnetosheath for Revolution 6 are shown in Figure 15. Although the polar cusp spectrum

may be noticeably deficient in lower energy electrons with $E \leq 800$ eV relative to the magnetosheath spectrum, this effect may be an artifact of the temporal variability of the electron spectrums as noted above. The high-latitude outer zone electron spectrums are readily distinguishable from the magnetosheath electron spectrums. These outer zone spectrums are broad and are usually characterized with a maximum of differential intensities at electron energies $\sim$ several keV.

Mid-altitude polar cusp structure.

The directional, differential intensities of low-energy protons and electrons within and in the vicinity of the polar cusp for Revolution 6 are shown in expanded scale in Figure 16. A persistent feature of all of these mid-altitude crossings of the polar cusp is the division of magnetosheath proton and electron intensities into two sheets. These two sheets are shaded in Figure 16. The low-energy electron sheet has so far always been observed to occur directly adjacent to and equatorward of the proton sheet which we have used to define the polar cusp. A crude estimate of the current density, due to protons and electrons in these regions (cf. Figures 11 and 15) yields $\sim 2 \times 10^8$ $(cm^2\text{-sec})^{-1}$ for both electrons and protons down the field

line. Since the latitudinal widths of these regions are roughly similar, these proton and electron sheets may well represent a downward flowing current and its upward return current, respectively. However, this does not account for the formation of two sheets at the mid-altitude polar cusp, one of magnetosheath proton intensities immediately adjacent to a sheet of the magnetosheath electron intensities. The latitudinal dimensions of these sheets, or bands, of proton and electron intensities as projected down to auroral altitudes would be $\sim$ 10 to 30 km.

V. Summary of Observations

First observations of the low-energy proton and electron intensities within the dayside polar magnetosphere have been presented here. Several of the more important observational results are:

- the polar neutral 'points' which appear at the high-latitude magnetopause in mathematical models for the shape of the geomagnetic cavity formed by the interaction of the solar wind with the geomagnetic field are observationally 'bands' with width $\sim$ 1 R_E across the dayside high-latitude magnetopause (one 'band' in the Northern hemisphere and presumably a second in the Southern hemisphere),

- these two 'bands', or regions of the magnetopause through which the magnetosheath plasma has direct access to the magnetosphere, and the corresponding extension of these bands from magnetopause to auroral altitudes have been designated herein as the 'polar cusps' (see Figure 9 for the geometry of the Northern polar cusp in the local-noon meridional plane),

- at all other positions of the dayside magnetopause, the magnetopause appears to be an effective barrier against the direct entry of magnetosheath plasma,

- during periods of relative magnetic quiescence the intersection of the dayside polar cusp with the auroral zone is positioned at invariant latitude $\Lambda = 79° (\pm 1°)$ and its latitudinal width is 10 to 30 km projected onto the auroral zone,

- during periods of relative magnetic disturbance the position of the polar cusp moves equatorward by several degrees in invariant latitude without a large increase in its latitudinal width, i.e., by factors ≤ 2,

- the high-latitude termination of energetic trapped electron ($E > 45$ keV) intensities in the high-latitude dayside outer radiation zone occurs coincident with the polar cusp, albeit these intensities are small and of irregular profile with radial distance in this region (see Figure 3),

- no measurable intensities of energetic electrons ($E > 40$ keV), magnetosheath protons and electrons, and ring-current protons were observed at latitudes above the polar cusp, i.e., in the polar cap region,

- the proton and electron differential energy spectrums as viewed in the solar direction in the distant polar cusp (within several earth radii of the magnetopause) are identical to those observed within the magnetosheath to within observational accuracy,

- the bulk velocity of protons in the distant polar cusp as deduced from the angular distributions appears to be lower than that of the magnetosheath plasma near the magnetopause by factors ~ 2 or 3,

- in the mid-altitude polar cusp at ~ 4 to 5 R_E geocentric radial distances, the proton spectrum differs from that at the magnetosheath in that protons with energies ≤ 500 eV are severely less than those observed in the magnetosheath,

- the proton spectrums in the mid-altitude polar cusp are similar to those in the distant plasma sheet with the exception that the proton number densities in the polar cusp are typically larger by factors $\sim$ 20 to 200,

- the angular distributions of proton intensities in the mid-altitude polar cusp are strongly peaked along the local magnetic field (i.e., down into the auroral zone); the dimensions of the atmospheric loss cone at these altitudes appear to be insufficiently large to account for the observed anisotropy, and

- the magnetosheath plasma in the mid-altitude polar cusp is observed to be separated into two thin sheets, one of magnetosheath proton intensities and the other populated with magnetosheath electrons; these sheets are immediately adjacent to each other with the electron sheet equatorward of the proton sheet; their latitudinal widths as projected into the auroral zone are roughly equal, $\sim$ 10 to 30 km.

VI. Implications of the Observed Polar Cusp Plasmas Concerning Magnetospheric Models

The first observations of the plasmas in the polar cusp as summarized in the previous section allow us to advance the following conclusions concerning the distant magnetosphere and its connection with the auroral zone. The principal interpretive conclusions based on the observations are

- the proton and electron intensities in the plasma sheet in the distant geomagnetic tail enter the magnetosphere through the dayside polar cusps,
- the high degree of access that the magnetosheath plasma has to the magnetosphere through these broad dayside polar cusps implies that the magnetic field lines threading the polar cusps are directly connected to the field lines in the magnetosheath (i.e., that merging of field lines occurs in the vicinity of the polar cusps' intersection with the magnetopause and/or along the surface of the sunlit magnetopause),
- the polar cusp on the dayside of the magnetosphere is spatially connected to the plasma sheet in the magnetotail,
- the magnetic field lines that thread the polar cusps are convected with the plasma down the flanks of the magnetopause along the polar cusp into the plasma sheet,

- the magnetic field lines of the polar cap region are swept back into the magnetotail but do not pass through the plasma sheet in the magnetotail,
- the magnetic field lines which thread the distant plasma sheet beyond ~ 10 or 12 R_E geocentric radial distances are mapped into the auroral zone precipitation pattern at its high-latitude boundary and coincident with the narrow band of low-energy electron intensities observed at this boundary [cf. Frank and Ackerson, 1970]. (The latitudinal width of this 'band' at auroral altitudes is ~ 20 to 150 km, a small region relative to the overall auroral precipitation zone.), and
- merging in the plasma sheet at the magnetic neutral plane reconnects the geomagnetic field lines.

The convection pattern for the distant magnetosphere given by the above model is qualitatively similar to that proposed by Axford and Hines [1961]. For a discussion of pertinent magnetospheric models and of magnetic merging, the reader is referred to the review by Axford [1969]. The major new interpretive results gained from this initial survey of the polar magnetosphere are (1) plasma sheet protons gain access to the magnetosphere via the polar cusps (2) all magnetic field lines threading the distant plasma sheet beyond ~ 10 or 12 R_E were convected from the dayside polar cusps and (3) magnetic field lines in the polar cap region

of the magnetic tail do not merge or pass through the plasma sheet. A diagram of this model of the magnetosphere is shown in Figure 17. The local noon-midnight meridional plane and the magnetopause as viewed from local evening are shown in the top and bottom panels, respectively, of Figure 17. Two magnetic field lines, B and b, passing through the polar cusps near local noon are convected (with velocity V_c at the magnetopause) into the plasma sheet, B' and b', and are reconnected with subsequent convection toward the earth, B" and b". The subsequent motion of the field lines to the dayside magnetosphere can be assumed to be such as to duplicate the convection patterns in the inner magnetosphere as deduced by Brice [1967]. The role of the polar cusp with regards to magnetic field lines in the polar cap region is discussed in the figure caption for Figure 17. Magnetic field lines from the polar cap region in the magnetic tail do not pass through the plasma sheet and are <u>not</u> populated with plasma sheet or auroral particles. The high-latitude magnetotail is observationally a region of low-energy, $\sim$ 1 keV, and low density, $\sim 10^{-2}$ $(cm)^{-3}$, protons [cf. Kanbach and Frank, 1970; Frank, 1969]. These proton intensities are significantly lower than those of the plasma sheet proper; no persistent, measurable proton intensities in this energy range have been detected as yet in the

polar cap region. In the presently proposed model only the magnetic field lines within the plasma sheet pass through the high-latitude magnetotail.

With regards to the mapping of the magnetic field lines passing through the auroral zone onto the equatorial plane near local midnight, Vasyliunas [1970] has recently shown that the inner edge of the plasma sheet electron intensities [cf. Vasyliunas, 1968; Schield and Frank, 1970; Frank, 1970b] maps into the low-latitude boundary of auroral precipitation at $\sim$ 6 R_E geocentric radial distances. Hence, with the exception of the narrow band of low-energy electron intensities at the high-latitude boundary of auroral precipitation which is mapped into the distant plasma sheet lying beyond $\sim$ 10 or 12 R_E we conclude that the auroral precipitation zone near local midnight is mapped into the equatorial plane over the radial distance range $\sim$ 6 to 10 or 12 R_E during periods of relative magnetic quiescence. The radial distance of $\sim$ 10 R_E approximately corresponds to the outer boundary of the extraterrestrial ring-current near local midnight as reported by Frank [1970b] or, equivalently, the radial distance for the onset of a significant increase of proton energy densities with decreasing radial distance in the plasma sheet. Further, if the magnetic field topology as de-

duced above is substantially correct, it appears that, for the most part, the Vela satellite measurements of plasmas at $\sim$ 18 R_E in the magnetotail correspond to the narrow band of low-energy electron intensities at the high-latitude boundary of the nighttime auroral zone [cf. Hones et al, 1970].

Our current research is being directed toward the behavior of the polar cusp, plasma sheet and auroral zone plasmas during magnetic substorms. However, it should be fairly obvious to the reader that the presently proposed magnetospheric model can easily account for such phenomena as the poleward expansion of auroras, the initial thinning and subsequent expansion of the plasma sheet, and the formation of a new plasma sheet within a previous sheet with changes in the character of the plasma flowing into the polar cusps (i.e., velocity, density, temperature, etc.). Our results thus far on this subject are consistent with the principal features of the above magnetospheric model and will be published in the near future.

Appendix

Coordinates and Universal Times for IMP 5 crossings of the polar cusp in the dayside polar magnetosphere are tabulated below.

Revolution	Date, Universal Time (1969)	Magnetic latitude, λ_m	Geocentric radial distance, R, kilometers	Solar magnetospheric longitude, ϕ_{sm}
3	1 July 09:15 U.T.	57.2° to 58.1°	38,357 to 37,315	15.3°
4	4 July 16:39 to 17:37	67.1° to 73.3°	54,007 to 42,806	1.1°
5	8 July 03:37	68.3°	24,711	0.6°
6	11 July 11:42	67.4° to 68.8°	35,212 to 33,797	10.9°
7	14 July 20:04	67.4°	42,009	349.0°
8	18 July 06:04	67.9°	25,279	8.6°
9	21 July 12:20 to 13:45	60.0° to 73.5°	56,494 to 38,882	1.2°
10	24 July 23:20	68.5°	28,617	340.3°
11	28 July 07:04 to 07:30	53.8° to 59.9°	43,122 to 35,874	356.2°

Revolution	Date, Universal Time (1969)	Magnetic latitude, λ_m	Geocentric radial distance, R, kilometers	Solar magnetospheric longitude, ϕ_{sm}
13	4 August 00:40	53.4°	41,591	336.9°
14	7 August 10:11	71.0°	31,177	5.5°

Acknowledgements

This research was supported in part by the National Aeronautics and Space Administration under contract NAS5-9074.

References

Antonova, A. E., and V. P. Shabansky, On the particle motion in the magnetosphere disturbed by the solar wind, Moscow State University Res. Rep., 1968.

Axford, W. I., Magnetospheric convection, Rev. of Geophysics, 7, 421-459, 1969.

Axford, W. I. and C. O. Hines, A unifying theory of high-latitude geophysical phenomena and geomagnetic storms, Can. J. Phys., 39, 1433-1464, 1961.

Brice, N., Bulk motion of the magnetosphere, J. Geophys. Res., 72, 5193-5211, 1967.

Chapman, S., Idealized problems of plasma dynamics relating to geomagnetic storms, Rev. Mod. Phys., 32, 919-933, 1960.

Chapman, S. and V. C. A. Ferraro, A new theory of magnetic storms, Terrestrial Magnetism and Atmospheric Electricity, Vol. 36, 77, 171, 1931; Vol. 37, 147, 421, 1932; and Vol. 38, 79, 1933.

Frank, L. A., Initial observations of low-energy electrons in the earth's magnetosphere with OGO 3, J. Geophys. Res., 72, 185-195, 1967a.

Frank, L. A., Several observations of low-energy protons and electrons in the earth's magnetosphere with OGO 3, J. Geophys. Res., 72, 1905-1916, 1967b.

Frank, L. A., Further comments concerning low energy charged particle distributions within the earth's magnetosphere and its environs, Particles and Fields in the Magnetosphere, ed. by B. M. McCormac, Reinhold Publishing Co., New York, 320-331, 1969.

Frank, L. A., On the presence of low-energy protons ($5 \leqslant E \leqslant 50$ keV) in the interplanetary medium, J. Geophys. Res., 75, 707-716, 1970a.

Frank, L. A., On the relationship of the plasma sheet, ring current, trapping boundary and plasmapause near the magnetic equator and local midnight, J. Geophys. Res. (submitted for publication), 1970b.

Frank, L. A. and K. L. Ackerson, Observations of charged particle precipitation into the auroral zone, J. Geophys. Res. (submitted for publication), 1970.

Frank, L. A., N. K. Henderson, and R. L. Swisher, Degradation of continuous-channel electron multipliers in a laboratory operating environment, Rev. Sci. Instr., 40, 685-689, 1969.

Heikkila, W. J. and J. D. Winningham, Penetration of magnetosheath plasma to low altitudes through the dayside magnetospheric cusps, J. Geophys. Res. (accepted for publication), 1970.

Hones, E. W., J. R. Asbridge, S. J. Bame and S. Singer, Energy spectra and angular distributions of particles in the plasma sheet and their comparison with rocket measurements over the auroral zone, J. Geophys. Res. (accepted for publication), 1970.

Kanbach, G. W. and L. A. Frank, Measurements of low-energy protons in the earth's magnetic tail, J. Geophys. Res., (to be submitted), 1970.

Roederer, J. G., Quantitative models of the magnetosphere, Rev. of Geophysics, 7, 77-96, 1969; also U. of Denver Res. Rep., 1968.

Schield, M. A. and L. A. Frank, Electron observations between the inner edge of the plasma sheet and the plasmasphere, J. Geophys. Res., 75, 5401-5414, 1970.

Spreiter, J. R., A. Y. Alksne and A. L. Summers, External aerodynamics of the magnetosphere, Physics of the Magnetosphere, ed. by R. L. Carovillano, J. F. McClay and H. R. Radoski, D. Reidel Publishing Company, Dordrecht, Holland, 301-375, 1968.

Spreiter, J. R. and B. R. Briggs, Theoretical determination of the form of the boundary of the solar corpuscular stream produced by interaction with the dipole field of the earth, J. Geophys. Res., 67, 37-51, 1962.

Vasyliunas, V. M., A survey of low-energy electrons in the evening sector of the magnetosphere with OGO 1 and OGO 3, J. Geophys. Res., 73, 2839-2884, 1968.

Vasyliunas, V. M., Relation of the plasma sheet to the auroral oval, (abstract), EOS, 51, 814, 1970.

Figure Captions

Figure 1. Directional, differential intensities of protons and electrons as functions of geocentric radial distance observed with the LEPEDEA on the satellite IMP 5 during an outbound pass through the magnetosphere near local noon and the magnetic equator on 11 July 1969. The directions for the fields-of-view of the detectors lie in the quadrant $225° \leq \phi_{SE} \leq 315°$ parallel to the ecliptic plane.

Figure 2. Selected geomagnetic coordinates for the series of observations shown in Figure 1 and the following Figure 3.

Figure 3. Continuation of Figure 1 for the inbound pass of IMP 5 through the polar magnetosphere near the local noon meridional plane on 11 July. Several coordinates as functions of geocentric raidal distance are given in Figure 2.

Figure 4. Summary of the observations of the plasma distributions within and near the magnetosphere in R - λ_m coordinates as observed during the inbound and outbound passes on 11 July (cf. Figures 1 and 3).

Figure 5. Summary of the positions of eleven polar cusp crossings in the dayside polar magnetosphere as functions of geocentric radial distance R and invariant dipole latitude Λ.

Figure 6. Comparison of several calculated positions of the polar cusp and of the neutral point at the magnetopause with the observed position in R - Λ coordinates.

Figure 7. Continuation of Figure 6 in R - λ_m coordinates.

Figure 8. A 'roadmap' for the various plasma regions encountered as functions of geocentric radial distance for six inbound passes through the dayside polar magnetosphere during periods of relative magnetic quiescence ($K_p < 2$). The passes have been ordered according to their latitude at 4.8 R_E, i.e., lowest latitude passes appear at the top of the diagram.

Figure 9. A diagram showing the geometry and location of the polar cusp within the polar magnetosphere in the noon meridional plane during periods of relative magnetic quiescence. The coordinates are geocentric radial distance R and dipole

magnetic latitude λ_m. The polar cusp intersects the auroral zone at $\Lambda \simeq 79°$. Several sample trajectories of IMP 5 through the dayside magnetosphere are also shown (cf. inbound passes with 'roadmap' of Figure 8).

Figure 10. Directional, differential spectrums of proton intensities in the solar direction for the distant polar cusp and the magnetosheath on 4 July as measured with the solar ion detector.

Figure 11. Directional, differential spectrums of proton intensities in the mid-altitude polar cusp and magnetosheath on 11 July. A proton spectrum for the distant plasma sheet within the magnetotail at 33.5 R_E as observed with IMP 4 on 6 February 1968 has been included for comparison.

Figure 12. Angular distributions of low-energy proton intensities for the distant polar cusp and the magnetosheath on 4 July.

Figure 13. Angular distributions of low-energy proton intensities as functions of local pitch angle α_d in the mid-altitude polar cusp on 24 July.

Figure 14. Directional, differential spectrums of electron intensities in the distant polar cusp and the magnetosheath on 4 July. The directions of the fields-of-view of the detector lie in a quadrant centered at $\phi_{SE} = 270°$.

Figure 15. Continuation of Figure 14 for the mid-altitude polar cusp, the high-latitude outer radiation zone and the magnetosheath on 11 July (see also Figure 3).

Figure 16. Detailed spatial distributions of low-energy proton and electron intensities in the vicinity of the mid-altitude polar cusp. The magnetosheath plasma is separated into two spatially adjacent sheets with the electron sheet positioned equatorward of the proton sheet.

Figure 17. Schematic diagram for the polar cusp-plasma sheet relationship in the magnetosphere. Main elements of this magnetospheric model are (1) plasma sheet protons gain access to the magnetosphere from the magnetosheath through the dayside polar cusps, (2) all magnetic field lines (B' and b') threading the distant plasma sheet beyond

10 or 12 R_E were convected from the dayside polar cusps, i.e., originally field lines B and b, (3) magnetic merging of geomagnetic field lines with magnetosheath field lines occurs along the polar cusps, (4) these geomagnetic field lines are reconnected , B" and b", in the neutral sheet within the magnetosphere and are convected toward the earth, (5) field lines B" and b" are subsequently convected into the dayside outer zone and (6) magnetic field lines in the polar cap region, C and D, do not merge in the magnetotail, are not populated with auroral particles and do not pass through the plasma sheet. In the dayside magnetosphere magnetic field lines of the polar cap region (C and D) and within the outer zone (A) at the magnetopause can merge with the field lines in the magnetosheath to form polar-cusp field lines (B and b). The model further assumes that field lines of the type B' and b' which do not merge at the neutral sheet become polar cap field lines C and D and provide the return of field

lines which were lost to the polar cap region at the dayside polar cusps. Field lines in the polar cap region (C and D) are connected to the field lines of the interplanetary medium. Thus the two distinct convection patterns in the model, polar cap and inner magnetospheric, are coupled via magnetic merging at the dayside polar cusps and in the neutral sheet in the magnetotail.

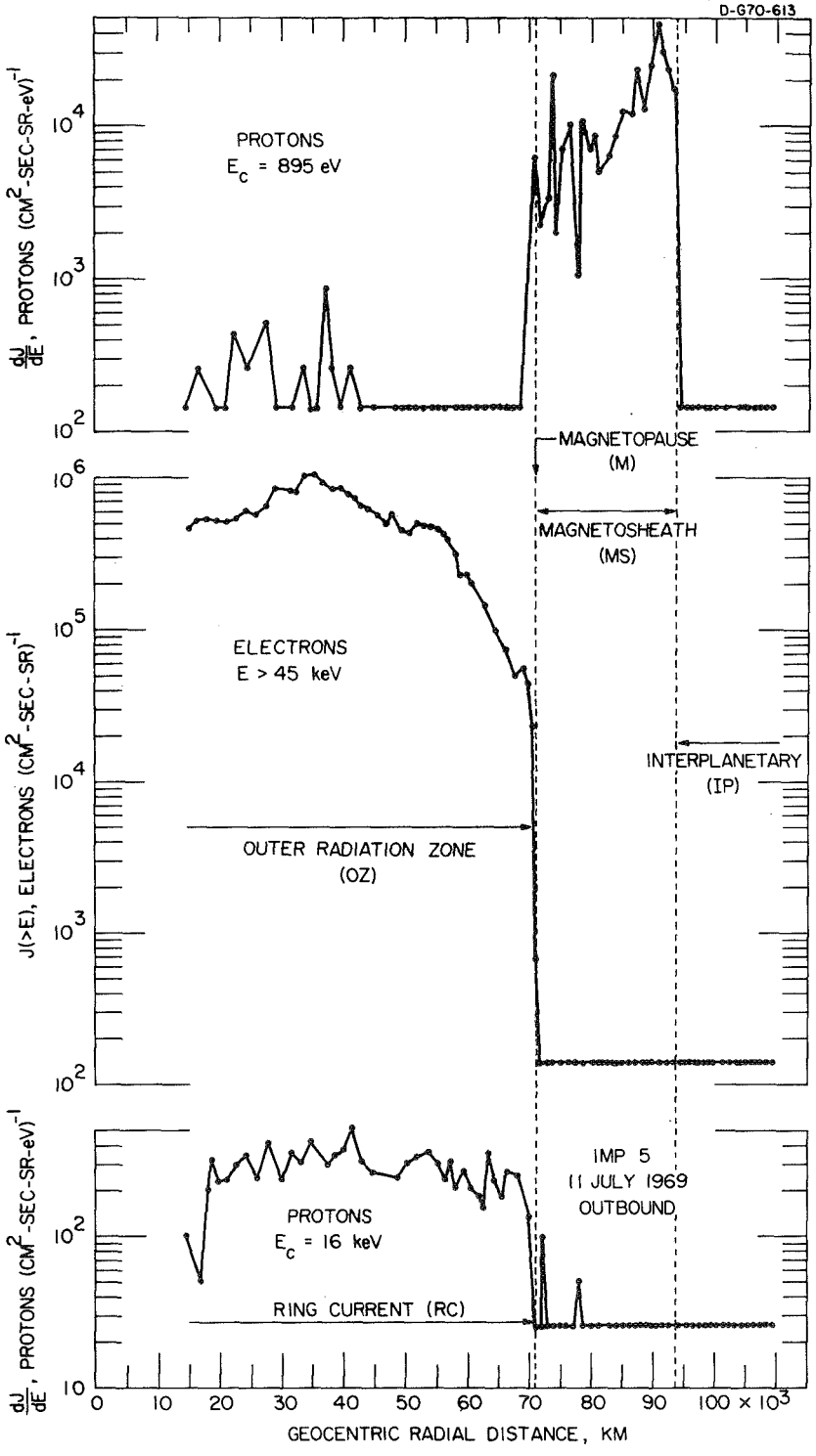
D-G70-613
PROTONS
E_c = 895 eV
$\frac{dJ}{dE}$, PROTONS (CM^2-SEC-SR-eV)$^{-1}$
MAGNETOPAUSE
(M)
MAGNETOSHEATH
(MS)
ELECTRONS
E > 45 keV
J(>E), ELECTRONS (CM^2-SEC-SR)$^{-1}$
INTERPLANETARY
(IP)
OUTER RADIATION ZONE
(OZ)
IMP 5
11 JULY 1969
OUTBOUND
PROTONS
E_c = 16 keV
RING CURRENT (RC)
$\frac{dJ}{dE}$, PROTONS (CM^2-SEC-SR-eV)$^{-1}$
GEOCENTRIC RADIAL DISTANCE, KM

Figure 1.

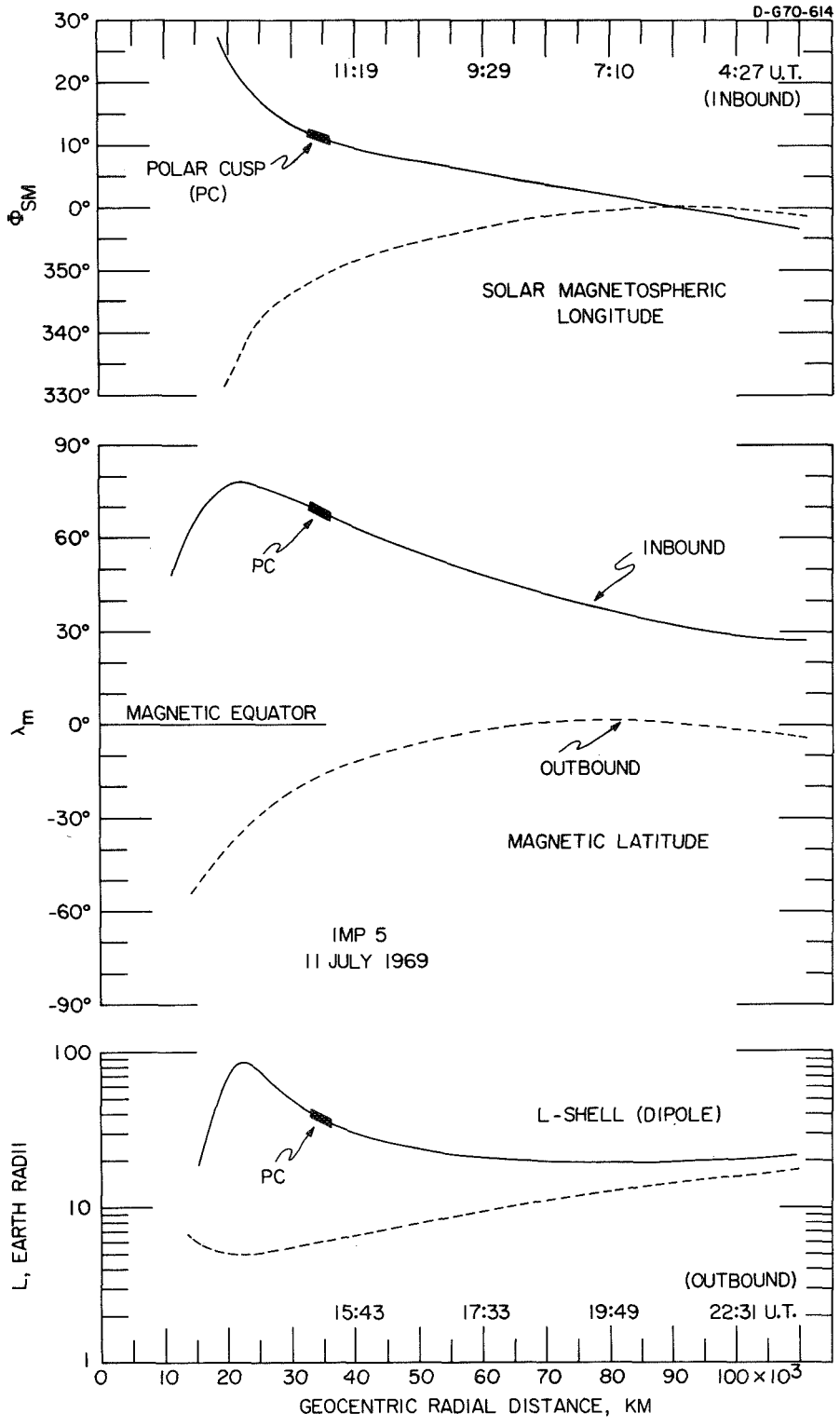
D-G70-614
30°
20°
10°
0°
350°
340°
330°
Φ_{SM}
11:19
9:29
7:10
4:27 U.T.
(INBOUND)
POLAR CUSP
(PC)
SOLAR MAGNETOSPHERIC
LONGITUDE
90°
60°
30°
0°
-30°
-60°
-90°
λ_m
PC
INBOUND
MAGNETIC EQUATOR
OUTBOUND
MAGNETIC LATITUDE
IMP 5
11 JULY 1969
100
10
1
L, EARTH RADII
L-SHELL (DIPOLE)
PC
(OUTBOUND)
15:43
17:33
19:49
22:31 U.T.
0
10
20
30
40
50
60
70
80
90
100×10³
GEOCENTRIC RADIAL DISTANCE, KM

Figure 2.

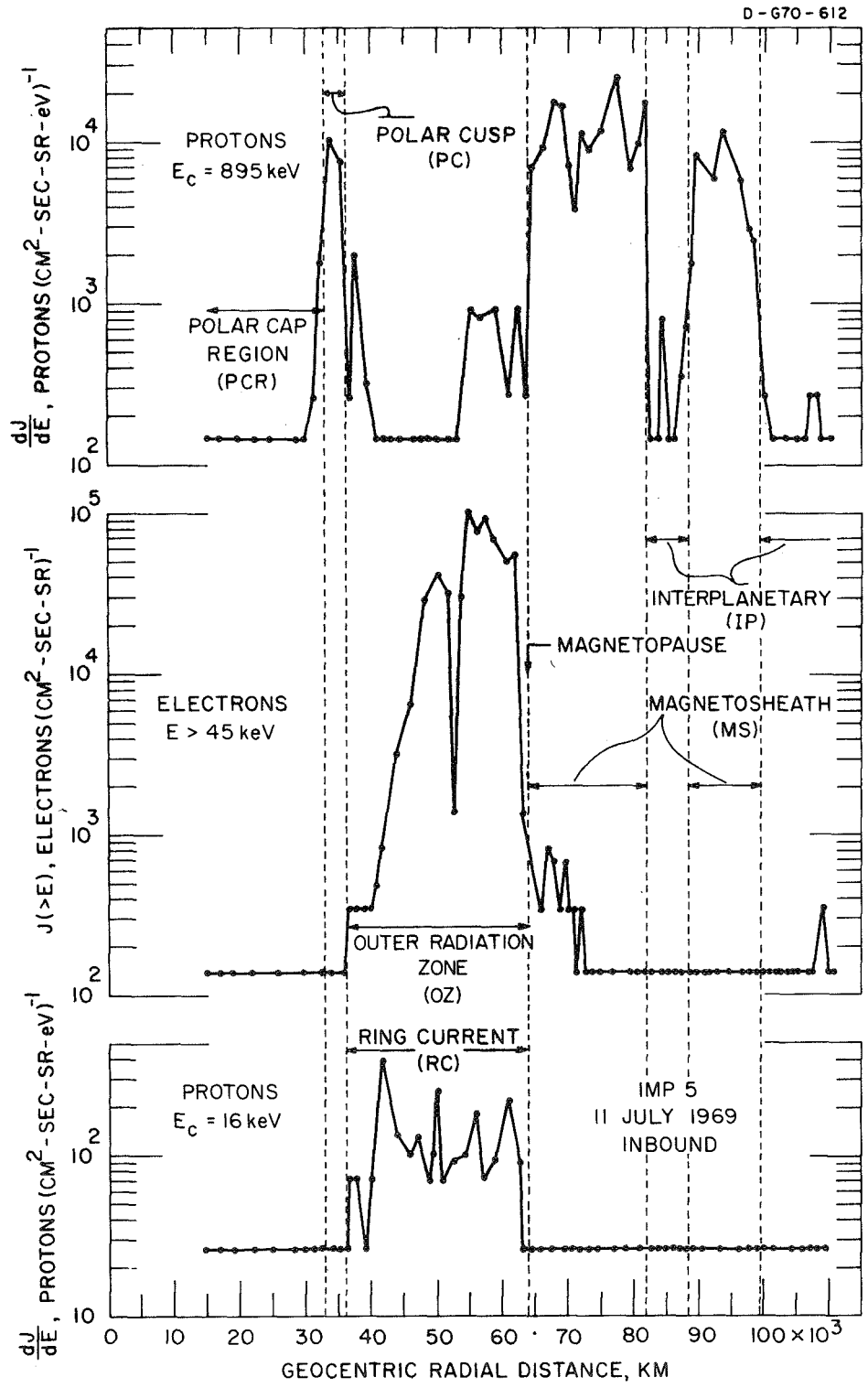
D-G70-612
PROTONS
E_c = 895 keV
POLAR CUSP
(PC)
POLAR CAP
REGION
(PCR)
$\frac{dJ}{dE}$, PROTONS $(CM^2\text{-}SEC\text{-}SR\text{-}eV)^{-1}$
ELECTRONS
E > 45 keV
INTERPLANETARY
(IP)
MAGNETOPAUSE
MAGNETOSHEATH
(MS)
OUTER RADIATION
ZONE
(OZ)
J(>E), ELECTRONS $(CM^2\text{-}SEC\text{-}SR)^{-1}$
RING CURRENT
(RC)
PROTONS
E_c = 16 keV
IMP 5
11 JULY 1969
INBOUND
$\frac{dJ}{dE}$, PROTONS $(CM^2\text{-}SEC\text{-}SR\text{-}eV)^{-1}$
0 10 20 30 40 50 60 70 80 90 100 × 10^3
GEOCENTRIC RADIAL DISTANCE, KM

Figure 3.

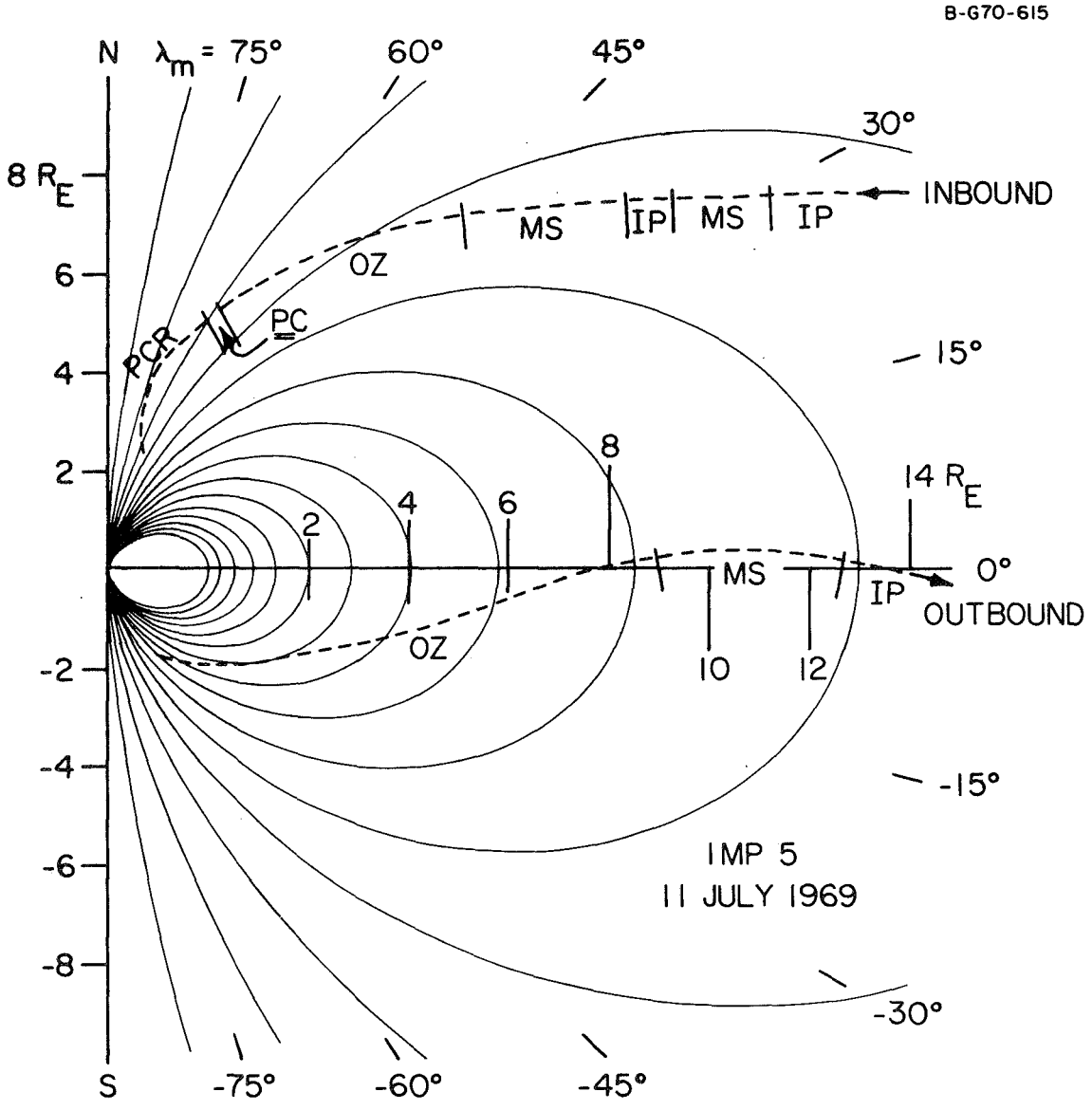
B-G70-615
N
λ_m = 75°
60°
45°
30°
8 R_E
6
4
2
-2
-4
-6
-8
INBOUND
MS
IP
MS
IP
OZ
PCR
PC
15°
8
14 R_E
4
6
2
MS
IP
0°
OUTBOUND
OZ
10
12
-15°
IMP 5
11 JULY 1969
-30°
S
-75°
-60°
-45°

Figure 4.

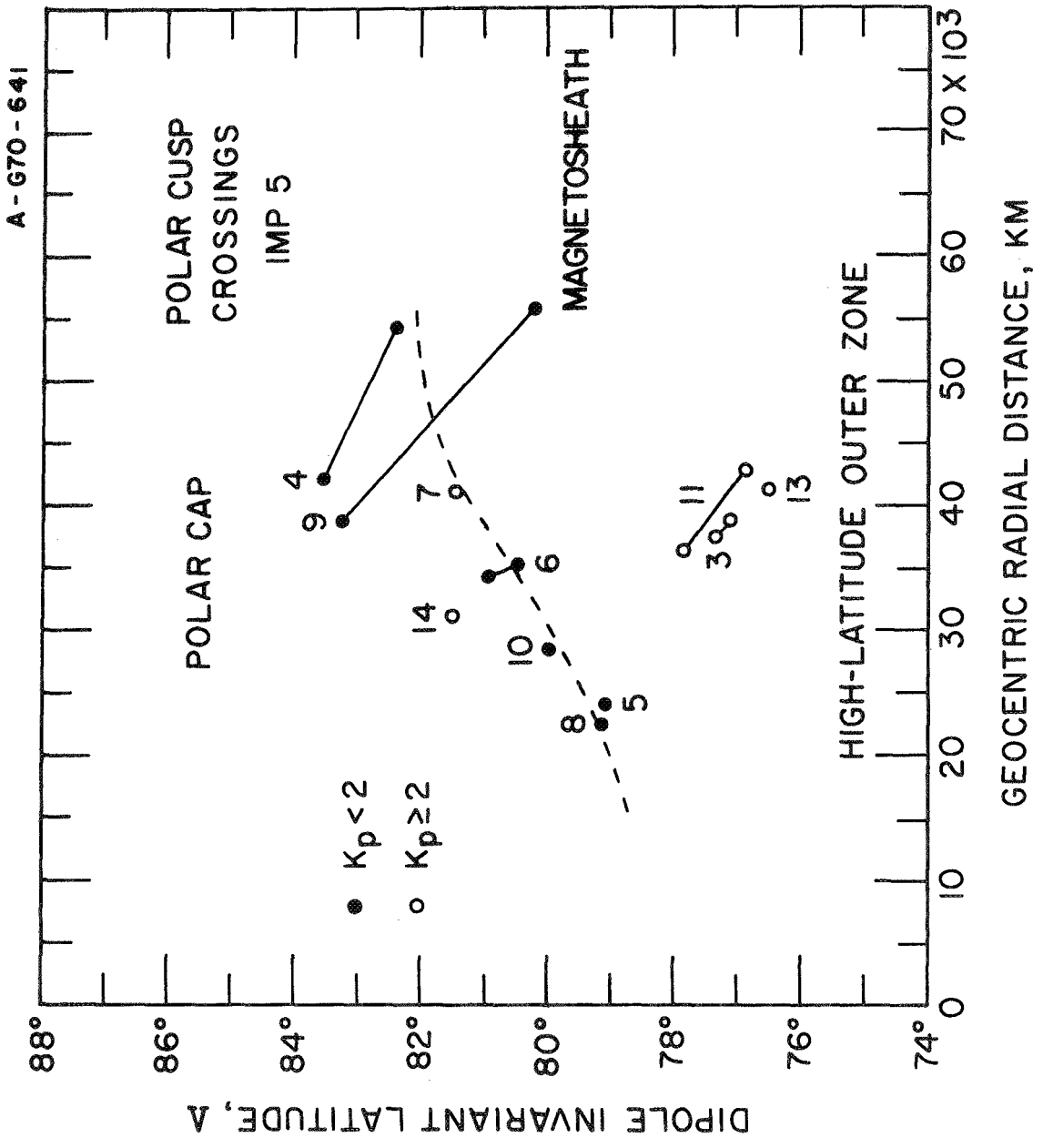
A-G70-641
POLAR CUSP
CROSSINGS
IMP 5
MAGNETOSHEATH
POLAR CAP
HIGH-LATITUDE OUTER ZONE
$K_p < 2$
$K_p \geq 2$
DIPOLE INVARIANT LATITUDE, Λ
88°
86°
84°
82°
80°
78°
76°
74°
0
10
20
30
40
50
60
70 X 103
GEOCENTRIC RADIAL DISTANCE, KM

Figure 5.

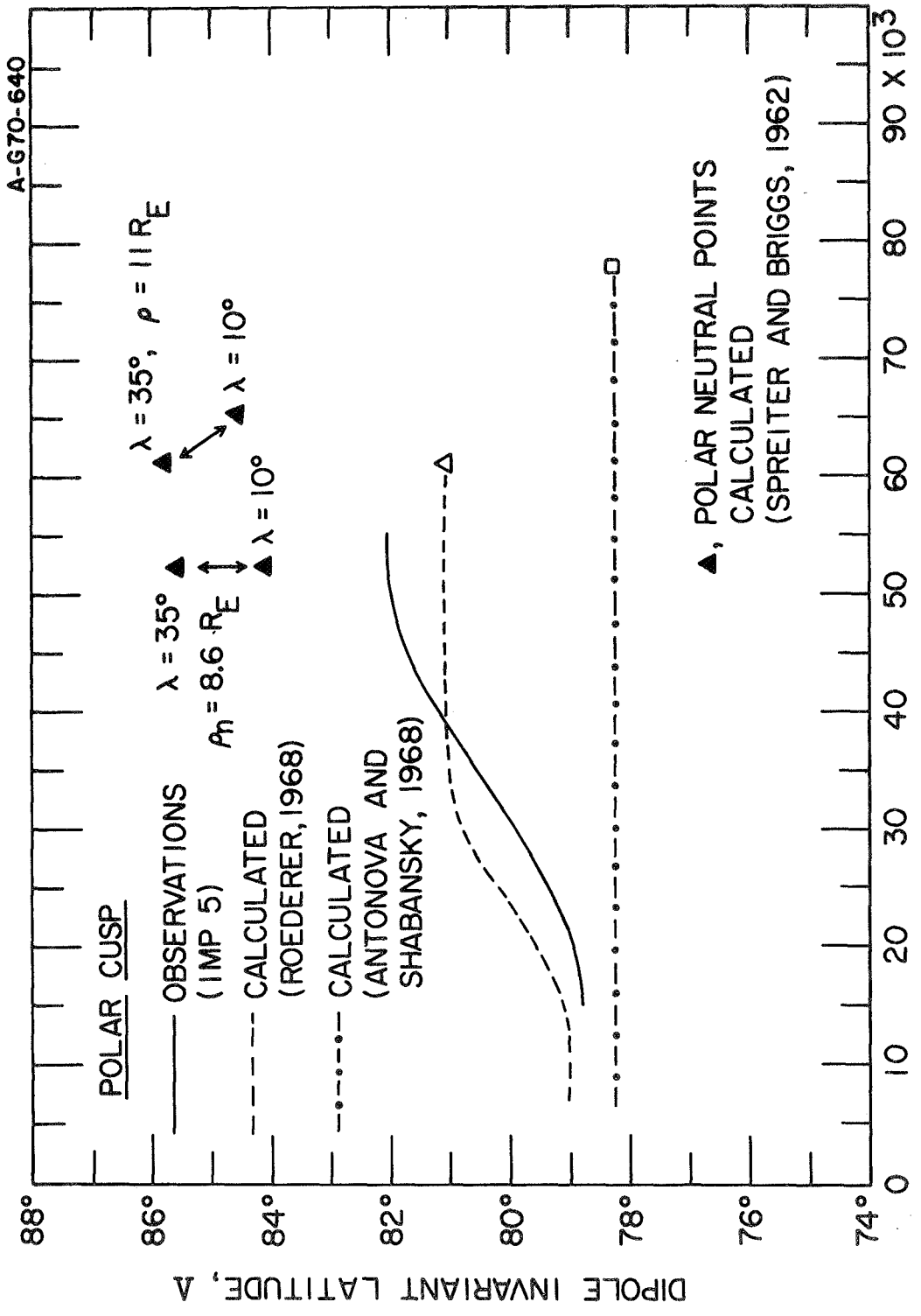
A-G70-640
POLAR CUSP
OBSERVATIONS (IMP 5)
CALCULATED (ROEDERER, 1968)
CALCULATED (ANTONOVA AND SHABANSKY, 1968)
λ = 35°
ρn = 8.6 RE
λ = 10°
λ = 35°, ρ = 11 RE
λ = 10°
▲, POLAR NEUTRAL POINTS CALCULATED (SPREITER AND BRIGGS, 1962)
DIPOLE INVARIANT LATITUDE, Λ
GEOCENTRIC RADIAL DISTANCE, KM
88°
86°
84°
82°
80°
78°
76°
74°
0
10
20
30
40
50
60
70
80
90 X 10³

Figure 6.

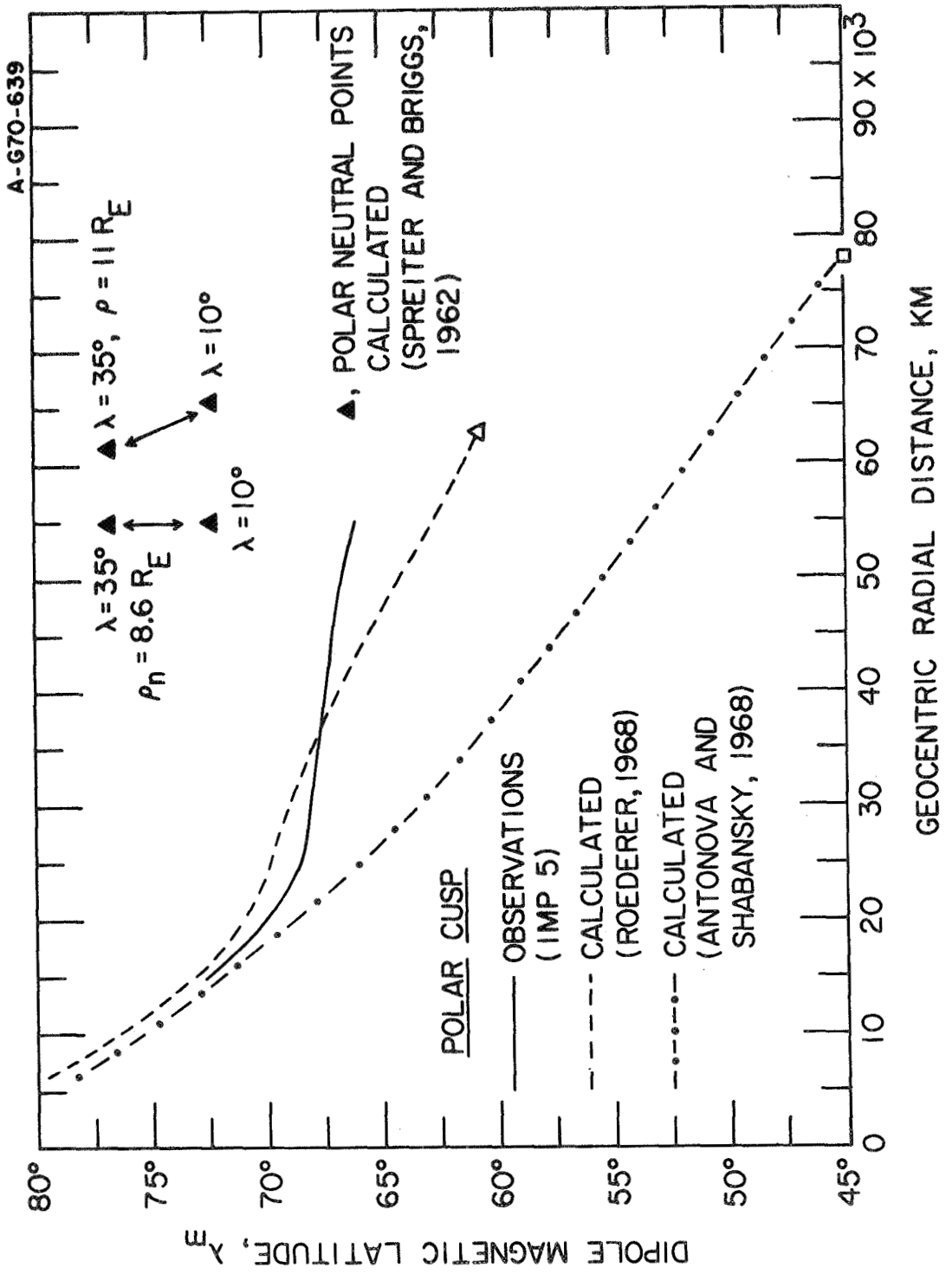
A-G70-639
DIPOLE MAGNETIC LATITUDE, λ_m
80°
75°
70°
65°
60°
55°
50°
45°
0
10
20
30
40
50
60
70
80
90 X 10^3
GEOCENTRIC RADIAL DISTANCE, KM
$\lambda = 35°$, $\rho = 11\ R_E$
$\lambda = 10°$
$\lambda = 35°$
$\rho_n = 8.6\ R_E$
$\lambda = 10°$
▲, POLAR NEUTRAL POINTS CALCULATED (SPREITER AND BRIGGS, 1962)
POLAR CUSP
OBSERVATIONS (IMP 5)
CALCULATED (ROEDERER, 1968)
CALCULATED (ANTONOVA AND SHABANSKY, 1968)

Figure 7.

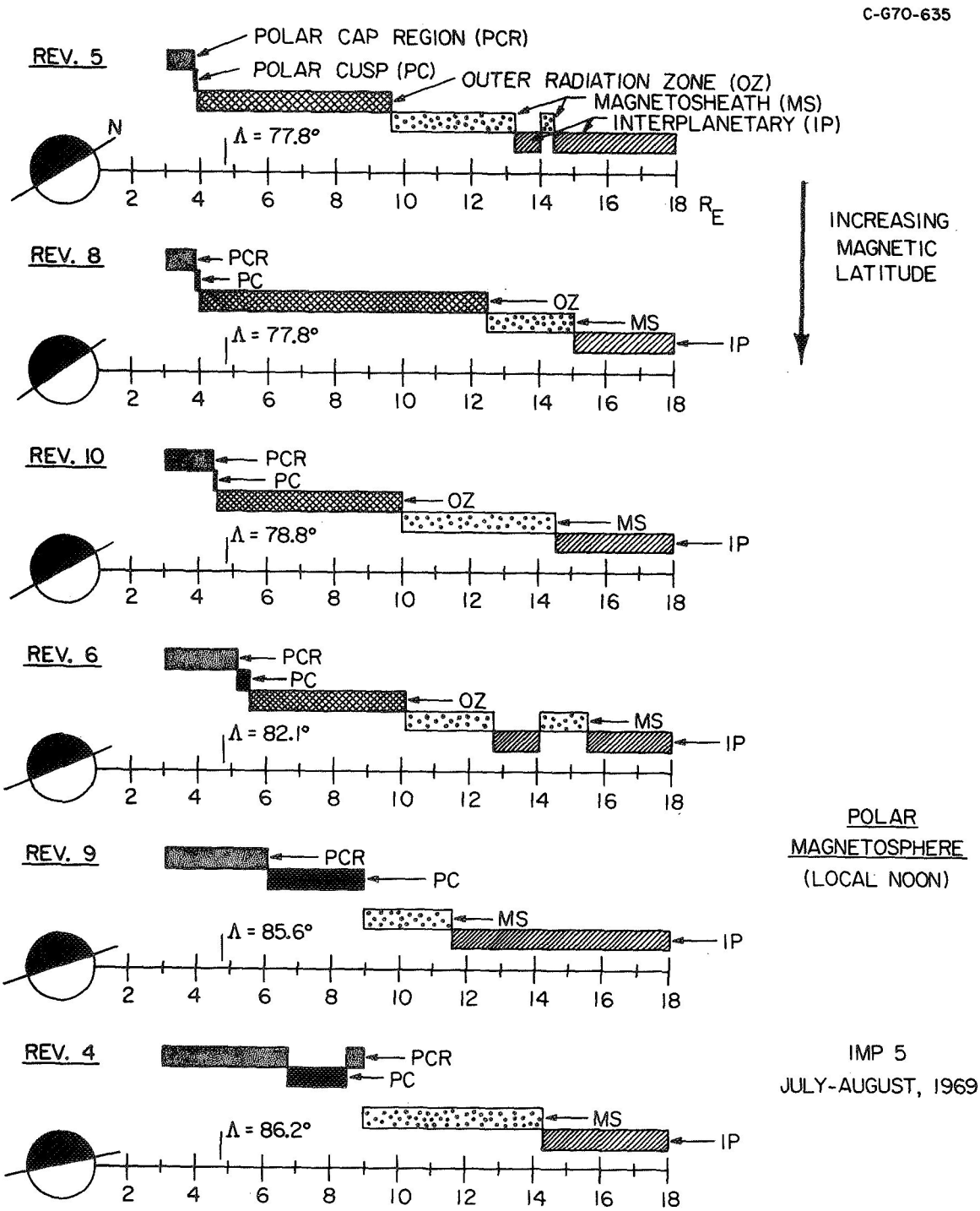
C-G70-635
REV. 5
POLAR CAP REGION (PCR)
POLAR CUSP (PC)
OUTER RADIATION ZONE (OZ)
MAGNETOSHEATH (MS)
INTERPLANETARY (IP)
N
Λ = 77.8°
2 4 6 8 10 12 14 16 18 R_E
INCREASING MAGNETIC LATITUDE
REV. 8
PCR
PC
OZ
MS
IP
Λ = 77.8°
2 4 6 8 10 12 14 16 18
REV. 10
PCR
PC
OZ
MS
IP
Λ = 78.8°
2 4 6 8 10 12 14 16 18
REV. 6
PCR
PC
OZ
MS
IP
Λ = 82.1°
2 4 6 8 10 12 14 16 18
POLAR MAGNETOSPHERE (LOCAL NOON)
REV. 9
PCR
PC
MS
IP
Λ = 85.6°
2 4 6 8 10 12 14 16 18
REV. 4
PCR
PC
MS
IP
Λ = 86.2°
2 4 6 8 10 12 14 16 18
IMP 5
JULY-AUGUST, 1969

Figure 8.

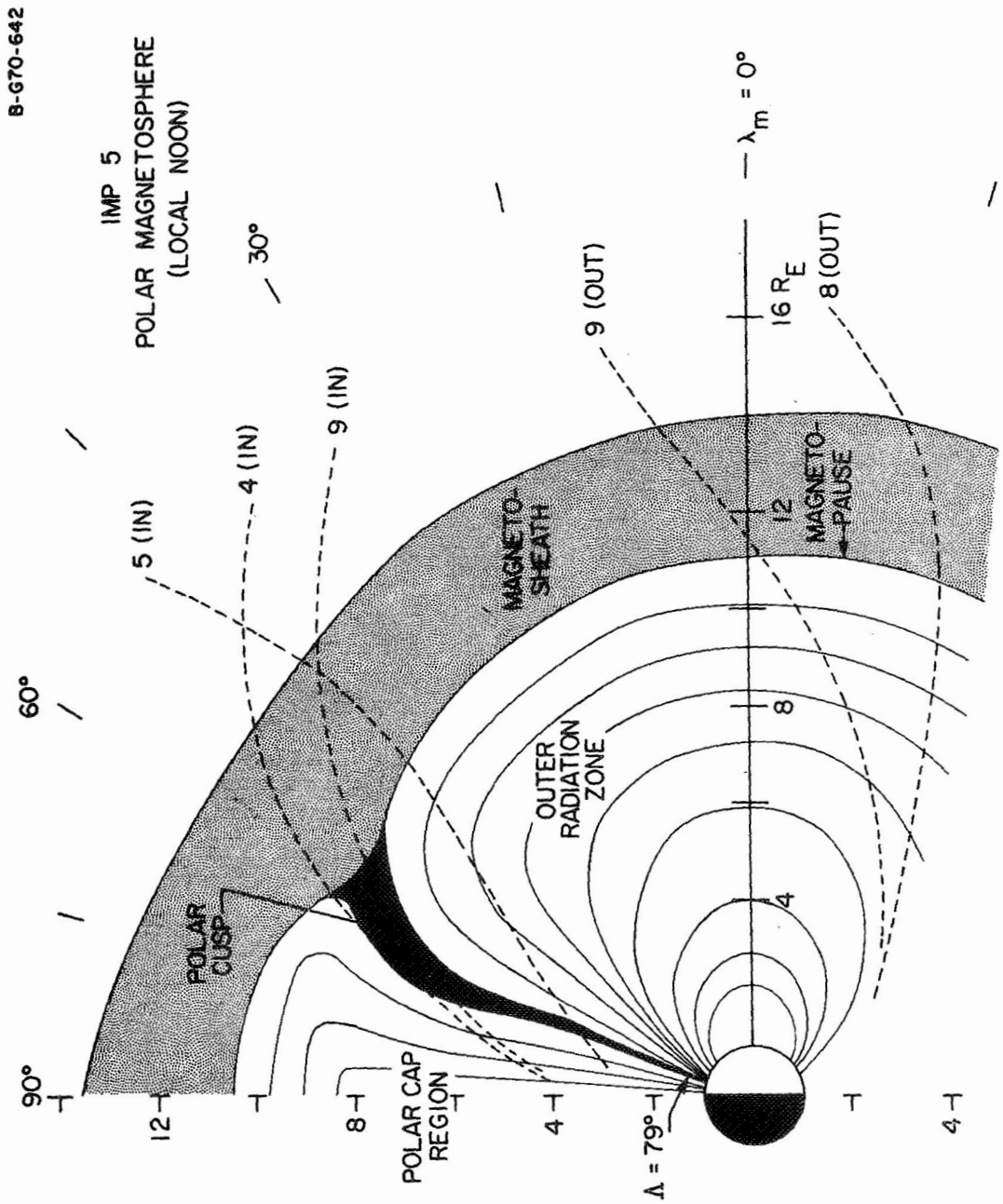
8-G70-642
IMP 5
POLAR MAGNETOSPHERE
(LOCAL NOON)
90°
60°
30°
-30°
$\lambda_m = 0°$
5 (IN)
4 (IN)
9 (IN)
9 (OUT)
8 (OUT)
16 R_E
12
MAGNETO-SHEATH
MAGNETO-PAUSE
POLAR CUSP
OUTER RADIATION ZONE
POLAR CAP REGION
$\Lambda = 79°$
12
8
4
8
4
4

Figure 9.

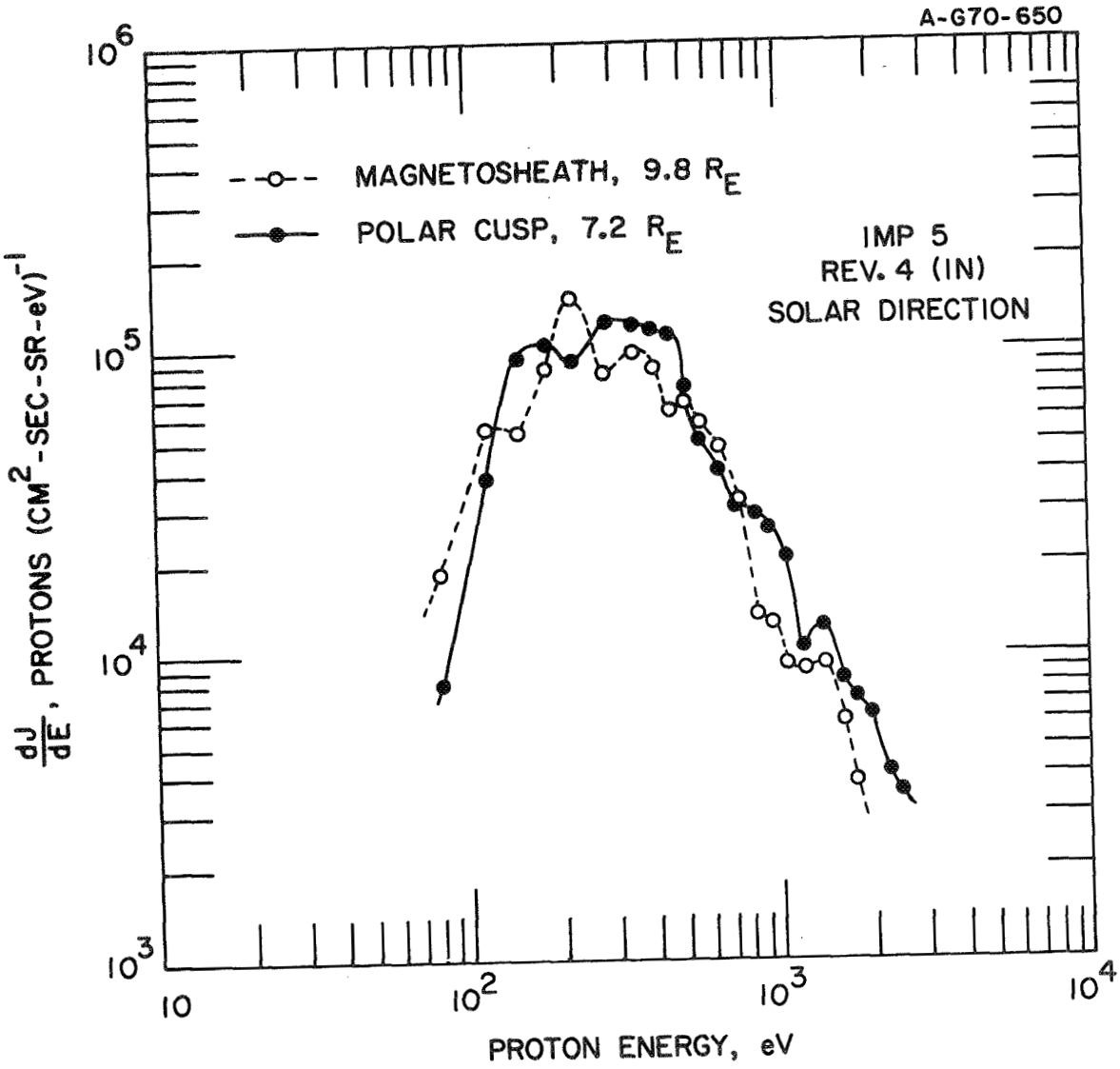
A-G70-650
MAGNETOSHEATH, 9.8 R_E
POLAR CUSP, 7.2 R_E
IMP 5
REV. 4 (IN)
SOLAR DIRECTION
$\frac{dJ}{dE}$, PROTONS $(CM^2\text{-}SEC\text{-}SR\text{-}eV)^{-1}$
10^6
10^5
10^4
10^3
10
10^2
10^3
10^4
PROTON ENERGY, eV

Figure 10.

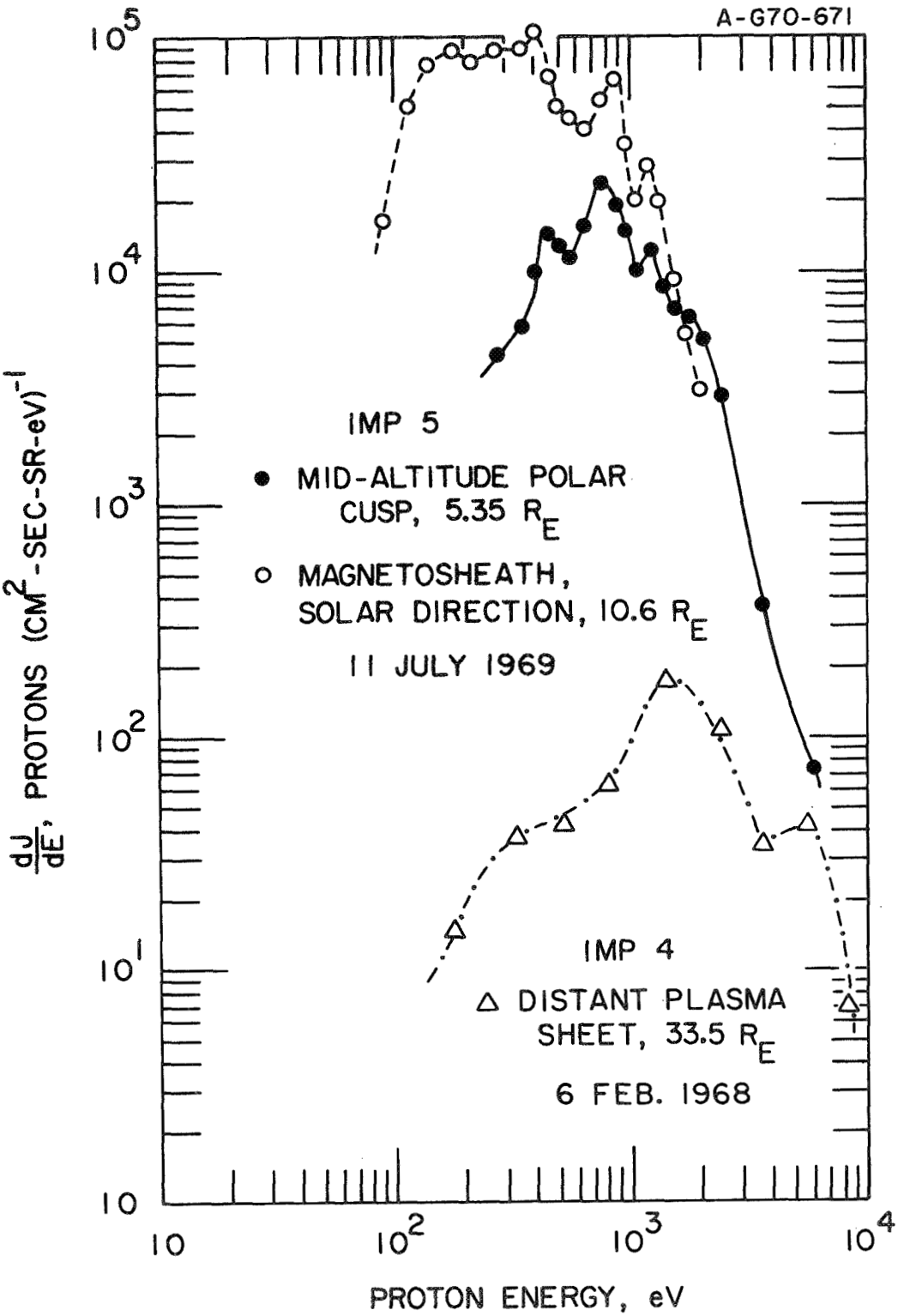
A-G70-671
IMP 5
MID-ALTITUDE POLAR CUSP, 5.35 R_E
MAGNETOSHEATH, SOLAR DIRECTION, 10.6 R_E
11 JULY 1969
IMP 4
DISTANT PLASMA SHEET, 33.5 R_E
6 FEB. 1968
$\frac{dJ}{dE}$, PROTONS $(CM^2\text{-SEC-SR-eV})^{-1}$
PROTON ENERGY, eV
10^5
10^4
10^3
10^2
10^1
10
10^2
10^3
10^4

Figure 11.

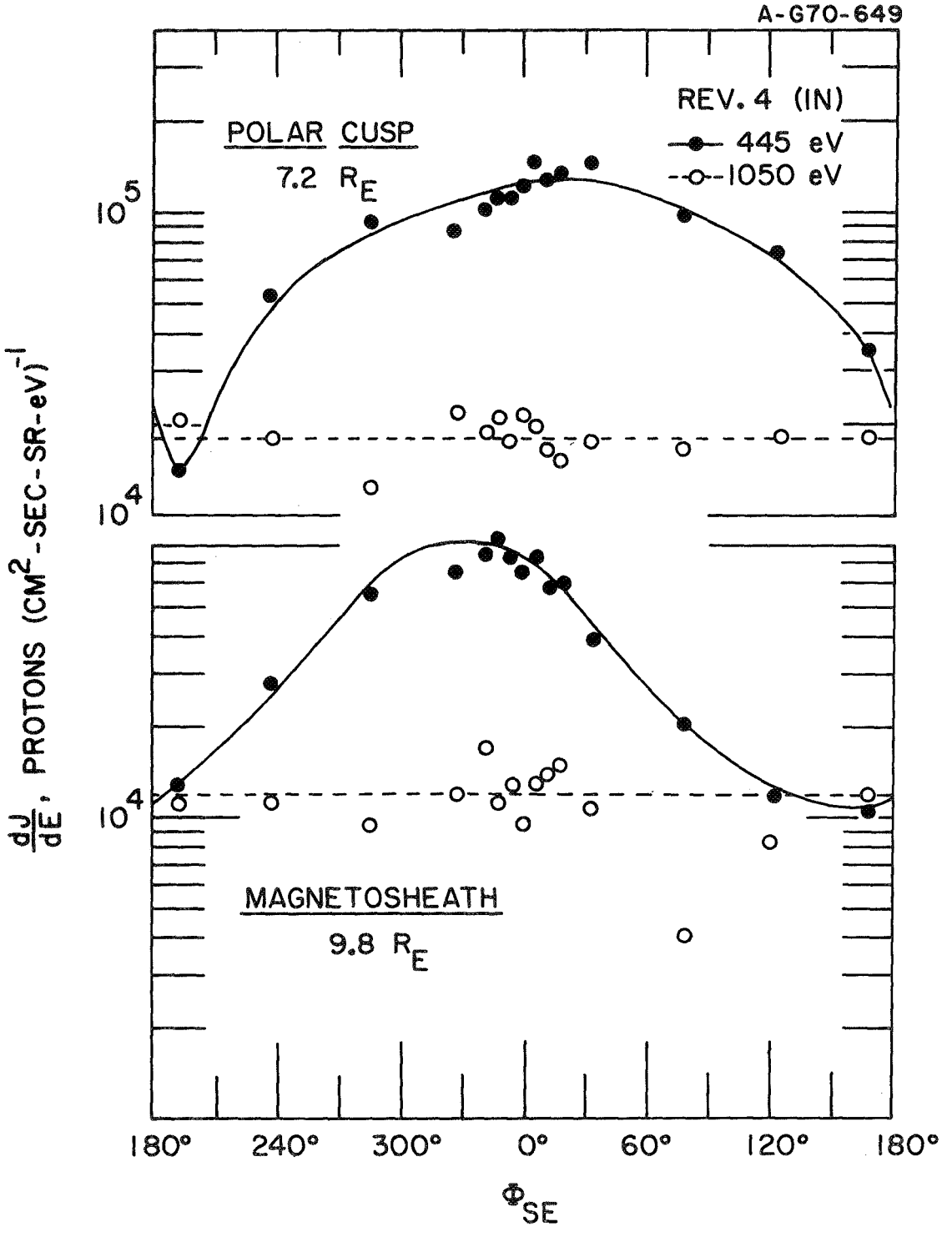
A-G70-649
REV. 4 (IN)
445 eV
1050 eV
POLAR CUSP
7.2 R_E
MAGNETOSHEATH
9.8 R_E
10^5
10^4
10^4
$\frac{dJ}{dE}$, PROTONS (CM^2-SEC-SR-eV)$^{-1}$
180°
240°
300°
0°
60°
120°
180°
Φ_{SE}

Figure 12.

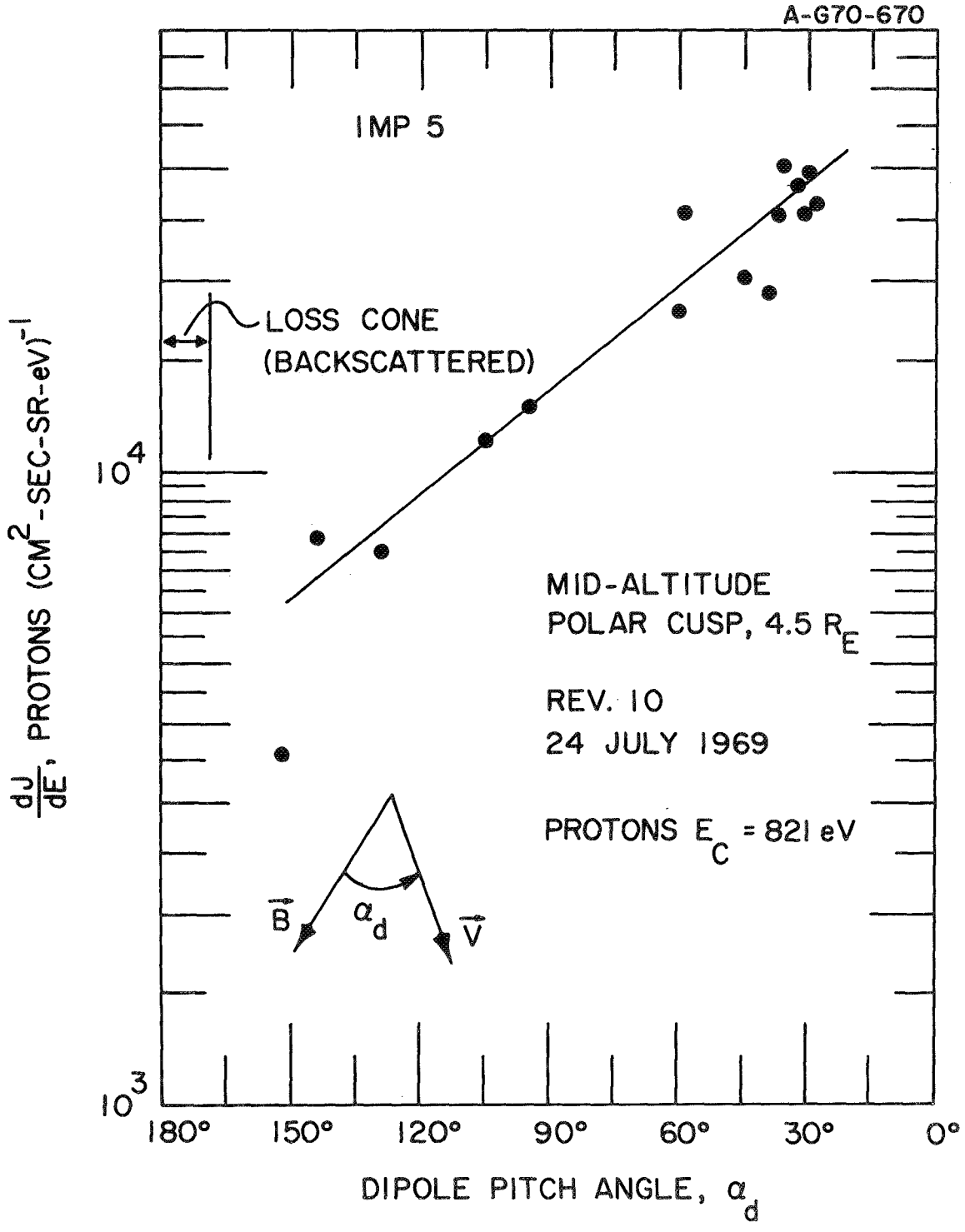
A-G70-670
IMP 5
LOSS CONE
(BACKSCATTERED)
MID-ALTITUDE
POLAR CUSP, 4.5 R_E
REV. 10
24 JULY 1969
PROTONS E_C = 821 eV
$\vec{B}$
α_d
$\vec{V}$
10^4
10^3
180°
150°
120°
90°
60°
30°
0°
$\frac{dJ}{dE}$, PROTONS (CM^2-SEC-SR-eV)$^{-1}$
DIPOLE PITCH ANGLE, α_d

Figure 13.

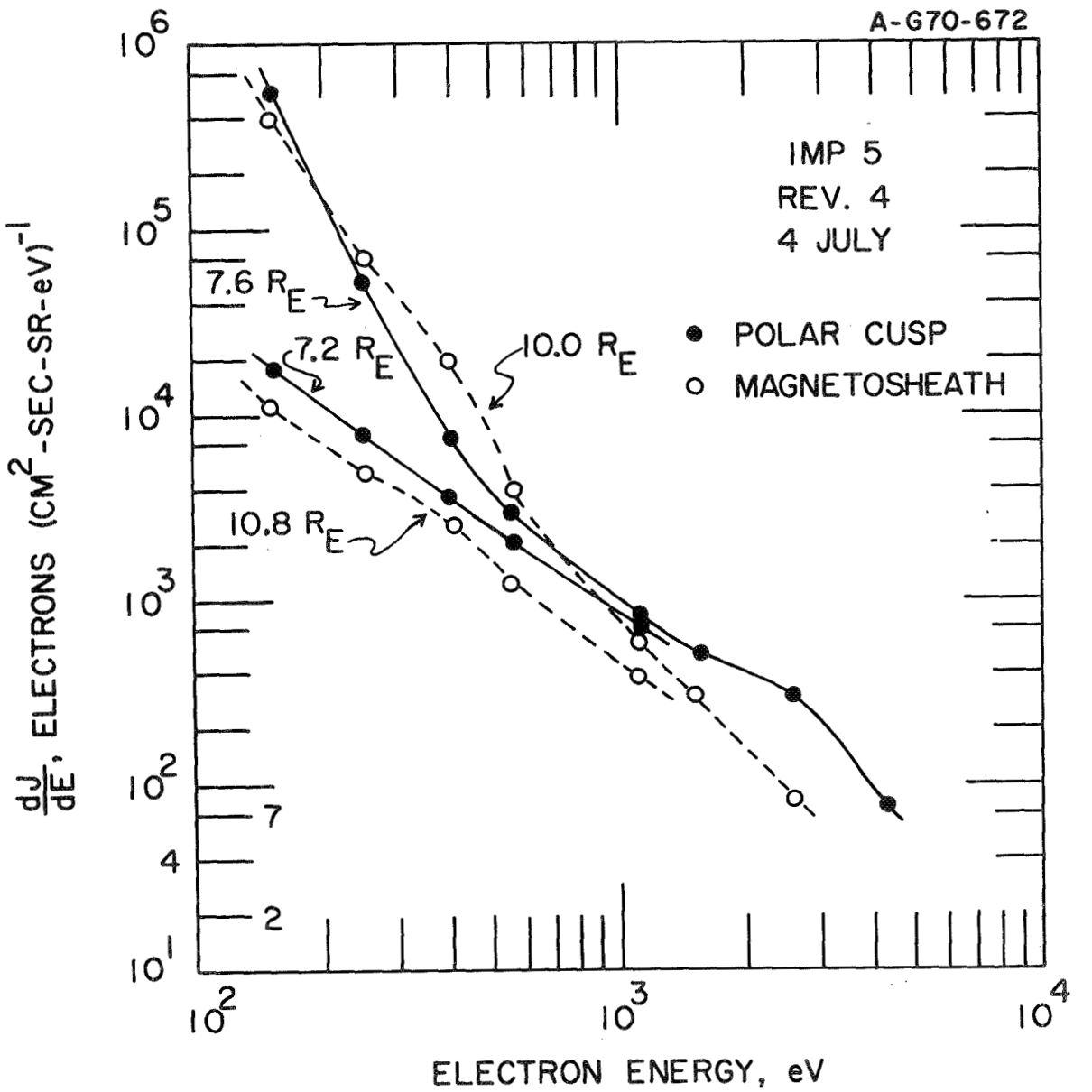
A-G70-672
IMP 5
REV. 4
4 JULY
POLAR CUSP
MAGNETOSHEATH
7.6 R_E
7.2 R_E
10.0 R_E
10.8 R_E
dJ/dE, ELECTRONS (CM^2-SEC-SR-eV)^-1
ELECTRON ENERGY, eV
10^6
10^5
10^4
10^3
10^2
10^1
7
4
2
10^2
10^3
10^4

Figure 14.

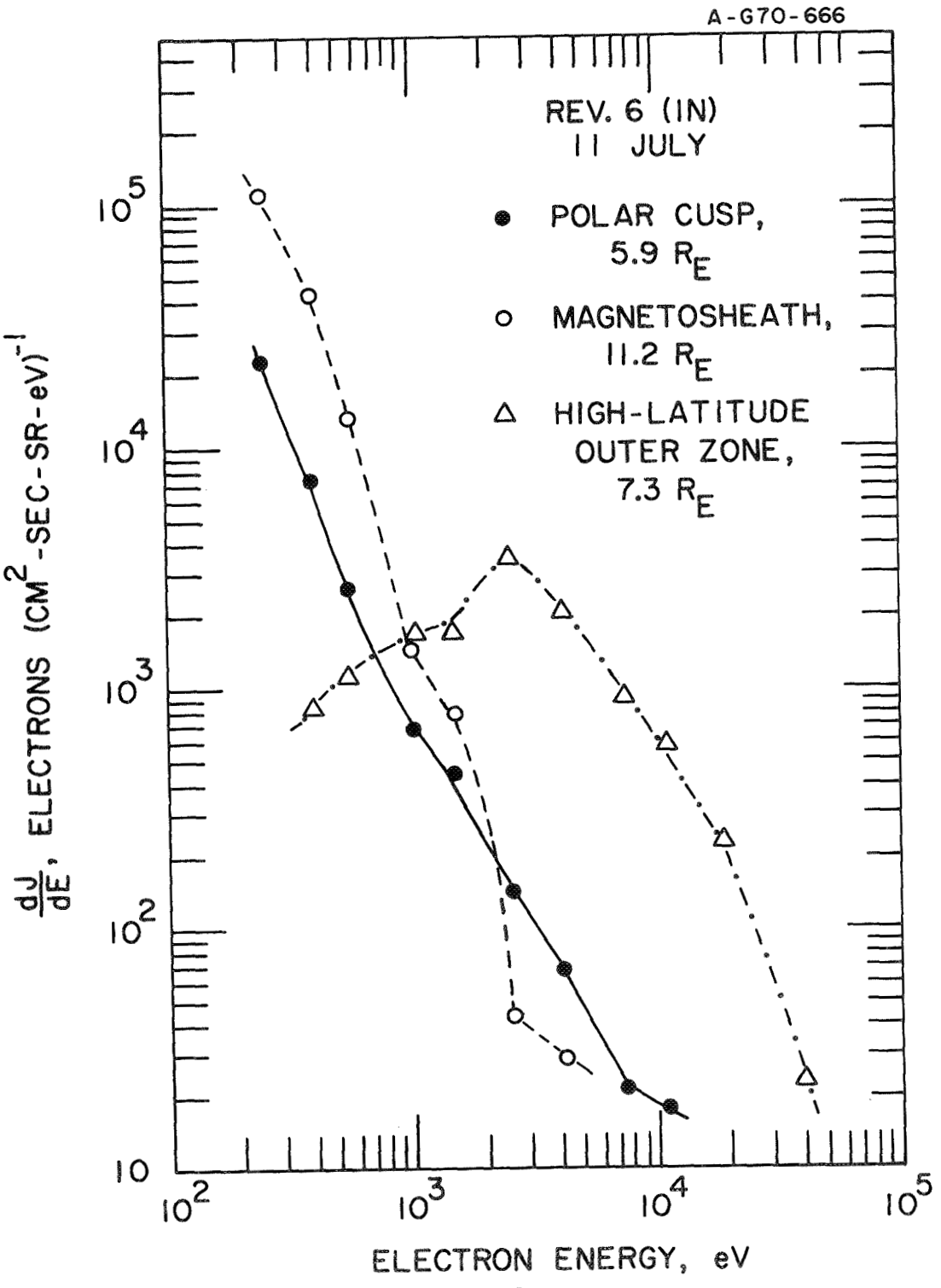
A-G70-666
REV. 6 (IN)
11 JULY
POLAR CUSP,
5.9 R_E
MAGNETOSHEATH,
11.2 R_E
HIGH-LATITUDE
OUTER ZONE,
7.3 R_E
$\frac{dJ}{dE}$, ELECTRONS (CM^2-SEC-SR-eV)$^{-1}$
10^5
10^4
10^3
10^2
10
10^2
10^3
10^4
10^5
ELECTRON ENERGY, eV

Figure 15.

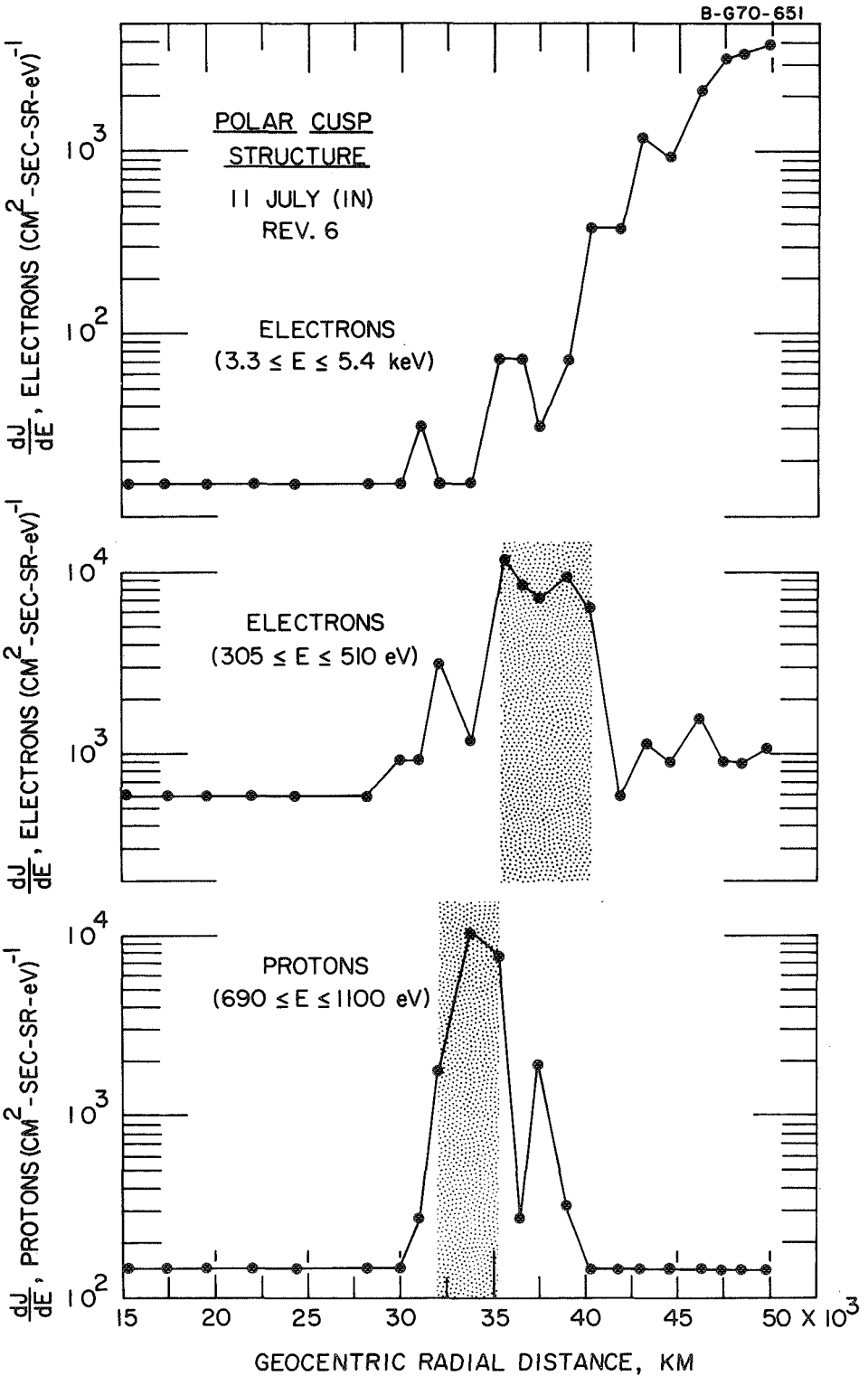
B-G70-651
POLAR CUSP
STRUCTURE
11 JULY (IN)
REV. 6
ELECTRONS
(3.3 ≤ E ≤ 5.4 keV)
ELECTRONS
(305 ≤ E ≤ 510 eV)
PROTONS
(690 ≤ E ≤ 1100 eV)
dJ/dE, ELECTRONS (CM²-SEC-SR-eV)⁻¹
dJ/dE, ELECTRONS (CM²-SEC-SR-eV)⁻¹
dJ/dE, PROTONS (CM²-SEC-SR-eV)⁻¹
10³
10²
10⁴
10³
10⁴
10³
10²
15
20
25
30
35
40
45
50 X 10³
GEOCENTRIC RADIAL DISTANCE, KM

Figure 16.

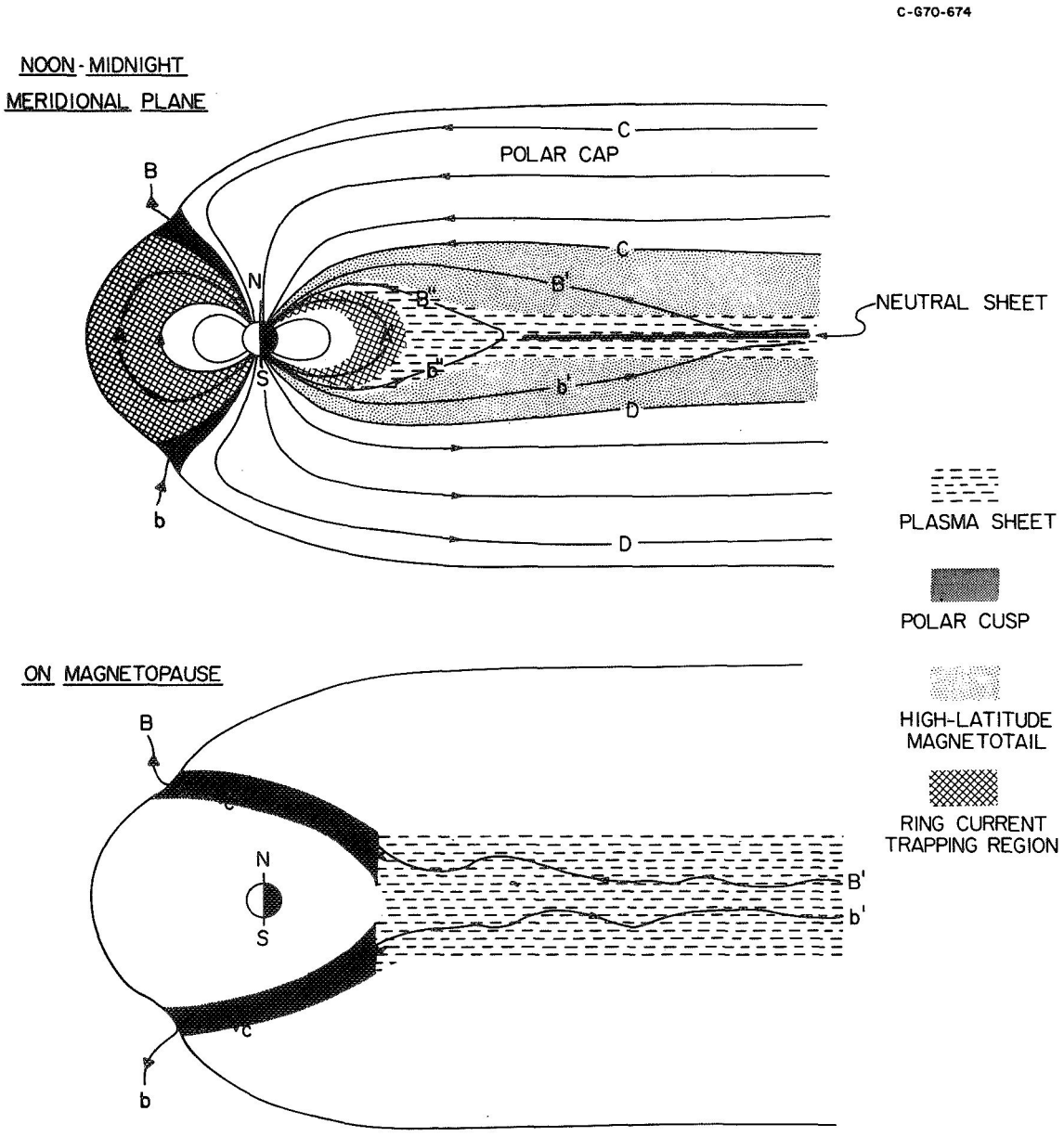

SCHEMATIC DIAGRAM FOR
POLAR CUSP - PLASMA SHEET RELATIONSHIP

Figure 17.